Article

Cell

The Nuclear Pore-Associated TREX-2 Complex Employs Mediator to Regulate Gene Expression

Graphical Abstract

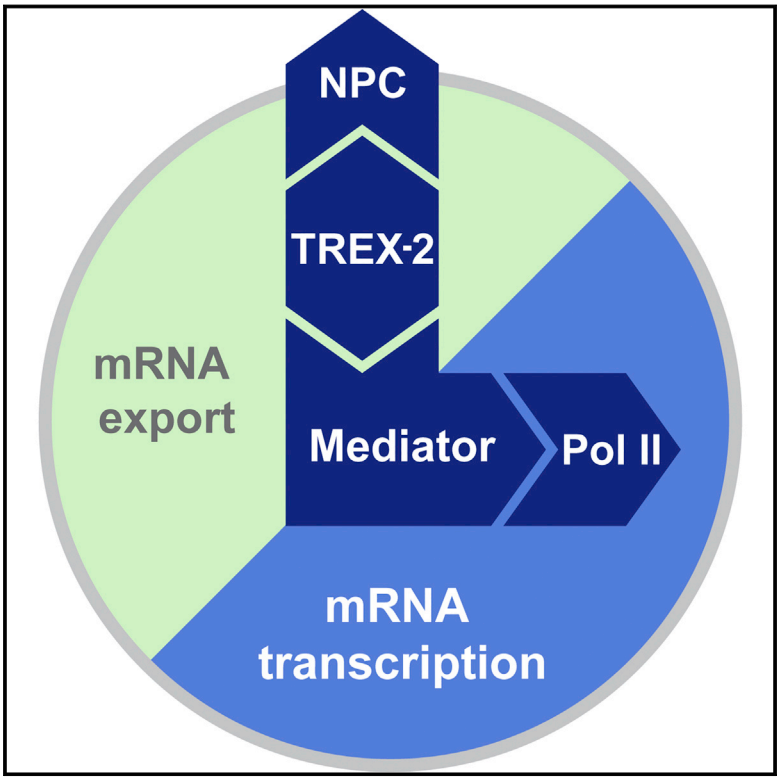

Authors

Maren Schneider, Doris Hellerschmied, Tobias Schubert, ..., B. Franklin Pugh, Tim Clausen, Alwin Köhler

Correspondence

alwin.koehler@mfpl.ac.at

In Brief

The NPC-associated TREX-2 complex directly interacts with Mediator, which in turn scaffolds RNA Pol II transcription initiation thus revealing how an NPC-associated adaptor complex accesses the core transcription machinery.

Highlights

- The nuclear pore-associated TREX-2 complex directly interacts with Mediator
- TREX-2 regulates Mediator association with Cdk8 and RNA Pol II Ser5 phosphorylation
- TREX-2 and the Med31 submodule co-regulate specific inducible and constitutive genes
- A similar TREX-2 surface promotes both transcription and mRNA export

Accession Numbers

4trq

Schneider et al., 2015, Cell *162*, 1016–1028
August 27, 2015
http://dx.doi.org/10.1016/j.cell.2015.07.059

CellPress

Cell

Article

The Nuclear Pore-Associated TREX-2 Complex Employs Mediator to Regulate Gene Expression

Maren Schneider,[1,4] Doris Hellerschmied,[2,4] Tobias Schubert,[1,4] Stefan Amlacher,[1] Vinesh Vinayachandran,[3] Rohit Reja,[3] B. Franklin Pugh,[3] Tim Clausen,[2] and Alwin Köhler[1,*]

[1]Max F. Perutz Laboratories, Medical University of Vienna, Vienna Biocenter Campus (VBC), Dr. Bohr-Gasse 9/3, 1030 Vienna, Austria

[2]Research Institute of Molecular Pathology, Dr. Bohr-Gasse 7, 1030 Vienna, Austria

[3]Department of Biochemistry and Molecular Biology, Center for Eukaryotic Gene Regulation, Pennsylvania State University, University Park, PA 16802, USA

[4]Co-first author

*Correspondence: alwin.koehler@mfpl.ac.at

http://dx.doi.org/10.1016/j.cell.2015.07.059

SUMMARY

Nuclear pore complexes (NPCs) influence gene expression besides their established function in nuclear transport. The TREX-2 complex localizes to the NPC basket and affects gene-NPC interactions, transcription, and mRNA export. How TREX-2 regulates the gene expression machinery is unknown. Here, we show that TREX-2 interacts with the Mediator complex, an essential regulator of RNA Polymerase (Pol) II. Structural and biochemical studies identify a conserved region on TREX-2, which directly binds the Mediator Med31/Med7N submodule. TREX-2 regulates assembly of Mediator with the Cdk8 kinase and is required for recruitment and site-specific phosphorylation of Pol II. Transcriptome and phenotypic profiling confirm that TREX-2 and Med31 are functionally interdependent at specific genes. TREX-2 additionally uses its Mediator-interacting surface to regulate mRNA export suggesting a mechanism for coupling transcription initiation and early steps of mRNA processing. Our data provide mechanistic insight into how an NPC-associated adaptor complex accesses the core transcription machinery.

INTRODUCTION

Nuclear pore complexes (NPCs) are both gateways for molecular transport and attachment sites for chromosomes. Genome-wide studies in yeast, flies, and humans have shown that nuclear pore proteins (nucleoporins) interact with numerous active genes, but also with heterochromatin boundaries and repressed genes (Ibarra and Hetzer, 2015). At present, the physical and functional connection between nucleoporins and the transcription machinery is poorly understood. A relay between nucleoporins and transcription could operate through an intermediate layer of adaptor proteins. Known candidates are the chromatin modifier SAGA (Köhler et al., 2008; Rodríguez-Navarro et al., 2004), the THO complex (Rougemaille et al., 2008), and the TREX-2 complex (Cabal et al., 2006). Specialized promoter elements (Ahmed et al., 2010) and the post-translational modification of transcription factors (Texari et al., 2013) further contribute to transient gene-NPC contacts. Given this complicated web of interactions, a key goal is to identify the functionally relevant NPC adaptors and to elucidate their molecular mechanisms of transcriptional control.

The conserved TREX-2 complex binds to the NPC basket structure (Fischer et al., 2004) and influences transcription and mRNA export (Gallardo et al., 2003), gene-NPC targeting (Cabal et al., 2006), DNA replication (Bermejo et al., 2011), and genome stability (González-Aguilera et al., 2008). This functional diversity is not understood on a mechanistic level. Earlier work reported dynamic, potentially indirect, interactions with promoter-bound co-activators like SAGA (Rodríguez-Navarro et al., 2004). Yeast TREX-2 consists of Sac3, Thp1, Sem1, Sus1, and Cdc31 and can be divided into a PCI domain part (a protein scaffold also found in the proteasome lid, CSN, and eIF3 complexes) and an NPC-anchor element (Figure 1A). A recent study revealed the structure of the PCI domains of Sac3 and Thp1 and the Sem1 protein (Ellisdon et al., 2012). This study also showed that TREX-2 binds to different nucleic acids in vitro and concluded that it may interact with RNA and/or DNA in vivo. However, the biological relevance of these interactions and their potential impact on transcription remained unclear. No specific interactions with any protein of the transcription machinery have been identified for the TREX-2 PCI domains.

Transcription initiation at eukaryotic protein-coding genes requires RNA Pol II, general transcription factors, and Mediator. Assembly of these factors on promoter DNA results in a core initiation complex, which recruits TFIIH to unwind DNA and phosphorylate the Pol II C-terminal domain (CTD). Mediator is recruited by transcription activators, stabilizes the initiation complex and stimulates TFIIH kinase activity (Poss et al., 2013). RNA synthesis leads to release of the general factors and formation of an elongation complex, which produces an mRNA nucleoprotein particle (mRNP) with a 5′ cap, 3′ poly(A)-tail and protein coat of various export factors. In the present work, we identify Mediator as a direct TREX-2 target and unravel a relay mechanism by which Mediator establishes the communication between TREX-2 and Pol II.

RESULTS

A Distinct Functional Region within the TREX-2 PCI Domain Core Complex

We hypothesized that the ability of TREX-2 to regulate both transcription and mRNA export is encoded in its PCI portion that represents the evolutionary most conserved part of the complex. Among PCI proteins two different types can be discerned: the TREX-2 subunit Thp1 contains a "typical" PCI, whereas Sac3 contains a less common "atypical" PCI, which features an additional N-terminal extension (Pick et al., 2009). Multiple sequence alignments of Sac3 revealed a conserved region (Sac3 aa 200–300), which corresponds to the atypical PCI extension (Figure S1A). Despite being highly conserved, this region was not functionally characterized in a recent study reporting the crystal structure of the yeast Sac3(253–551)/Thp1/Sem1 complex (PDB: 3t5v) (Ellisdon et al., 2012). To address the function of the most conserved region of Sac3 we determined the crystal structure of a *Saccharomyces cerevisiae* TREX-2 sub-complex containing an N-terminally extended variant of Sac3 (Sac3(222–572)/Thp1(170–455)/Sem1) at 3.1 Å resolution revealing an overall organization that was highly similar to the reported structure (root-mean-square deviation [rmsd] values: Sac3 0.8 Å, Thp1 1.4 Å, and Sem1 2.8 Å for 299, 450, and 56 equivalent Ca atoms, respectively) (Figure 1B). Despite their conservation, Sac3 residues 222–252 were not defined by electron density, most likely because this segment is inherently flexible. Strikingly, mapping the sequence conservation onto the TREX-2 PCI structure highlighted a distinct surface patch in the atypical part of the Sac3 PCI domain as the largest conserved region of the entire Sac3/Thp1/Sem1 complex (Figure 1C). This region includes Sac3 helices α1, α2, and α4 and consists of two clusters of positively charged residues centered around R256 and R288 (Figure 1D). To analyze the function of this region, we phenotypically characterized the impact of point mutations in residues that are identical between yeast and human (Figures 1E and S1A). Interestingly, both *sac3 R256D* and *R288D* mutations, exhibited pronounced growth defects with the *R288D* mutation being more severely affected on galactose-containing medium, a condition that requires highly inducible transcription of the NPC-targeted *GAL1* gene (Figure 1E). The respective alanine substitutions resulted in weaker phenotypes, while other mutations (e.g., *D351R*) showed no readily detectable growth defects. The observed phenotypes do not result from Sac3 protein instability, as the mutant proteins assembled into stable complexes with the other TREX-2 subunits (Figures S1B and S1C) and localized to NPCs in vivo (Figure S1D). Sac3 residues K467 and K468, located in the remote winged helix subdomain, were reported to be crucial for nucleotide binding and mRNA export (Ellisdon et al., 2012). However, upon mutation (*sac3 K467D/K468D*) we detected comparatively minor growth phenotypes under the conditions of our assay, consistent with these residues being poorly conserved (Figures S1A and S2A). Thus, our analysis assigns a critical function to the N-terminal region of the atypical Sac3 PCI domain.

TREX-2 Affects Mediator Composition and Preinitiation Complex Assembly

To address the role of the Sac3 PCI domain in transcription, we reasoned that it might influence the formation of the preinitiation complex, a multi-protein assembly at gene promoters, which includes RNA Pol II, the general transcription factors and Mediator. As potential TREX-2 interactors, we considered factors with a known capacity to respond to external signals. In yeast and metazoa, Mediator is the key "processor," which binds transcription factors, facilitates preinitiation complex assembly, recruits Pol II, and releases it into elongation (Flanagan et al., 1991; Poss et al., 2013; Thompson et al., 1993). Yeast Mediator contains 25 subunits arranged in four modules designated as "head," "middle," "tail," and "kinase" (Figure 2C) (Poss et al., 2013) and interacts with Pol II over a large surface area. The kinase is a tetrameric module comprising the Cdk8 enzyme, its activator CyclinC, Med12, and Med13 (Borggrefe et al., 2002; Liao et al., 1995). The Cdk8 kinase module (CKM), among other functions regulates the interconversion between active and repressive forms of Mediator (Poss et al., 2013).

Affinity-purification of the TAP-tagged Mediator subunit Med7 (part of the middle module) showed a characteristic Mediator subunit profile in wild-type cells (Figure 2A). Intriguingly, in *sac3*Δ cells, Mediator lost its Cdk8 kinase subunit as assessed by mass spectrometry and immunoblotting (Med13 and Med12 were also affected but to a lesser extent). The stoichiometry of other Mediator proteins was not markedly altered. Cdk8 levels were unchanged in *sac3*Δ cells (Figure 2A) and loss of Cdk8 was also seen when using TAP-tagged Med15 (tail) as bait for purification (Figure S2C). Together, these data suggest that TREX-2 affects the association of Mediator with its Cdk8 kinase module.

Mediator function is linked to multi-site phosphorylation of the Pol II C-terminal domain (CTD), a repetitive heptapeptide array ($YSPTSPS_{27}$) in the Rpb1 subunit. The CTD is thought to be largely unphosphorylated during preinitiation complex assembly (Robinson et al., 2012). Upon phosphorylation of Ser5 residues, Pol II escapes from the promoter and starts mRNA synthesis (Liu et al., 2004; Wong et al., 2014). Mediator itself can stimulate CTD phosphorylation (Plaschka et al., 2015; Søgaard and Svejstrup, 2007). To test whether TREX-2 has a regulatory influence on Pol II, we isolated Mediator and determined the total amount and phospho-status of the interacting Pol II (Figure 2B). We observed substantially less Pol II co-purifying with Mediator in *sac3*Δ cells when probing with an antibody against the CTD of Rpb1 (mAb clone 8WG16). Remarkably, this fraction of Pol II exhibited strongly increased Ser5 phosphorylation (Ser5-P) levels in *sac3*Δ cells when assayed with a site-specific antibody (mAb clone 4H8). The TREX-2-dependent increase in Pol II Ser5 phosphorylation was also detected in total cell extracts. On the other hand, Ser2 phosphorylation, a CTD mark that accumulates at the 3′ region of a gene, remained largely unchanged. These results were confirmed by directly purifying Pol II from wild-type and *sac3*Δ cells (Figure S2D). Taken together, our data indicate that TREX-2 is important for maintaining normal cellular levels of RNA Pol II Ser5-P and further suggest that the strongly increased Ser5 CTD phosphorylation may partially disrupt the interaction with Mediator as reported earlier (Søgaard and Svejstrup, 2007).

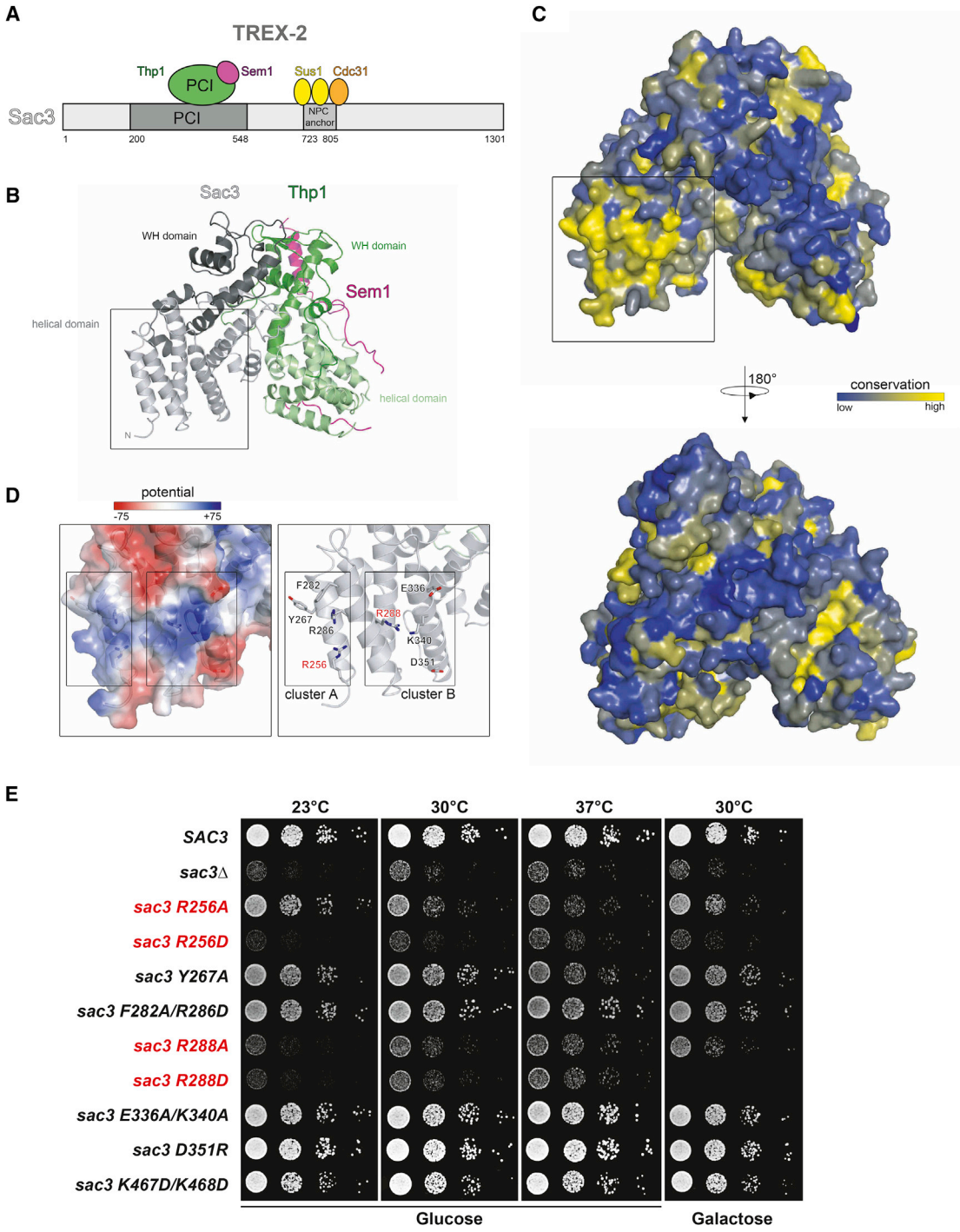

Figure 1. A Functionally Conserved Region on the TREX-2 PCI Domain

(A) Cartoon of the yeast TREX-2 domain organization. Sac3 domain boundaries are drawn to scale.

(B) Ribbon representation of the TREX-2 PCI domain complex with Sac3, Thp1 and Sem1 shown in gray, green, and magenta, respectively. The PCI domains of Thp1 and Sac3 consist of stacks of helical repeats each capped by a C-terminal winged-helix (WH) domain. Sem1 adopts an extended conformation, which grasps around and stabilizes the loosely packed protein scaffold of Thp1. Boxed region marks the N-terminal pole of the "atypical" Sac3 PCI domain.

(C) Front and back view of the complex showing its surface conservation. Conservation scores of the individual residues are represented by color gradients from blue (no conservation) to yellow (100% conservation). Scores were calculated based on multiple sequence alignments (see also Figure S1A). Boxed region corresponds to (B).

(legend continued on next page)

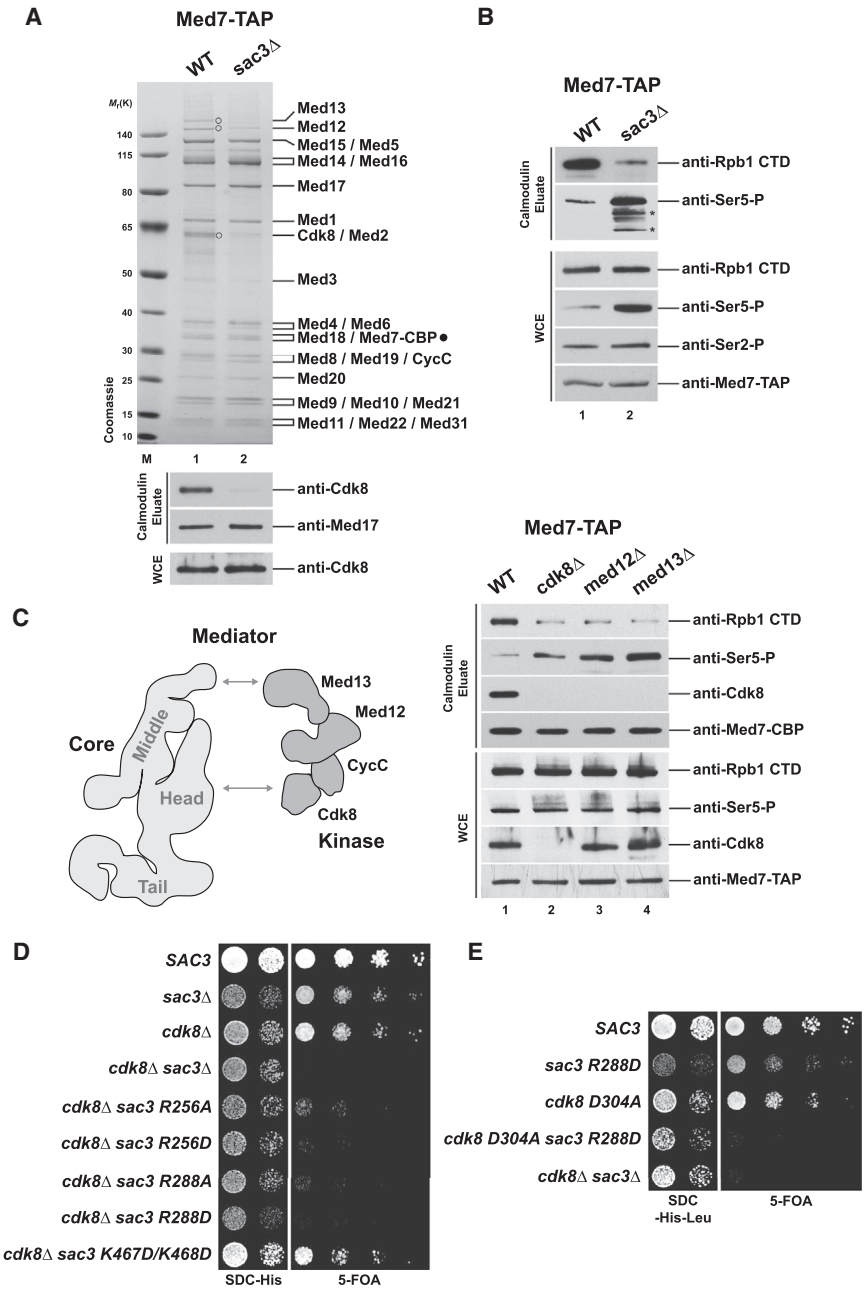

Figure 2. TREX-2 Affects Cdk8 Module Assembly with Mediator Core

(A) The yeast Mediator complex was affinity-purified via TAP-tagged Med7 from wild-type and *sac3Δ* cells. Calmodulin eluates were analyzed by SDS-PAGE and Coomassie staining (upper panel) and immunoblotting (lower panel). Assigned subunits were determined by mass spectrometry (bands were excised from gel). Note that the Cdk8 module proteins are present in substoichiometric amounts in wild-type Mediator preparations (labeled with open circles, except CycC, which co-migrates with other proteins). Immunodetection of Med17 was used for normalization. WCE, whole cell extract; M_r(K), molecular weight standard.

(B) The same purification as in (A) was further probed with the indicated antibodies. Asterisks indicate degradation products of Rpb1.

(C) Med7-TAP-purifications of Mediator from wild-type and mutant cells. Calmodulin eluates and whole cell extracts were immunoblotted with the indicated antibodies. See Figure S2E for corresponding Coomassie gel. Cartoon depicts the contours of the Mediator core (head, middle, tail) and Cdk8 module structures (both drawn to scale) based on cryo-EM data (Tsai et al., 2014). Arrows indicate contact points between the complexes (Tsai et al., 2014).

(D) Genetic interaction analysis. A *sac3Δ/cdk8Δ* shuffle strain containing a *SAC3* cover plasmid (URA3) was transformed with wild-type *SAC3*, empty vector, or the indicated *sac3* mutant alleles (HIS plasmids). Growth was followed on SDC-His (loading control) and on SDC+5-fluoroorotic acid (5-FOA) plates to shuffle out the URA cover plasmid.

(E) Same set-up as in (D) except that cells were co-transformed with wild-type *CDK8* or a *cdk8* catalytic point mutant.

See also Table S6.

TREX-2 and the Cdk8 Kinase Module Are Functionally Linked

Given that TREX-2 affects both Ser5 phosphorylation of Pol II and Cdk8 integration into Mediator, we explored the impact of the Cdk8 kinase module on Ser5 phosphorylation in vivo. Kin28 (human CDK7), a subunit of the general transcription factor TFIIH, is regarded as the main Ser5 CTD kinase. Human CDK8 was reported to inhibit CDK7 by phosphorylation (Akoulitchev et al., 2000), raising the possibility of a similar cross-talk in yeast. We isolated the Mediator complex from cells carrying deletions of *CDK8, MED12*, and *MED13* (see cartoon in Figure 2C). These deletions disrupted the Cdk8 kinase module (CKM) to

(D) The insets show helices α1–α4 of the Sac3 PCI domain and correspond to the boxed regions in (B) and (C). Electrostatic surface potential and ribbon representation highlight two clusters (A and B) of positively charged residues. R256 and R288 (labeled in red) are located in the center of cluster A and B, respectively. Residues analyzed in mutational studies are shown in stick mode.

(E) Growth analysis of wild-type *SAC3* and mutant strains on medium prepared with glucose or galactose. The *sac3Δ* strain was transformed with wild-type *SAC3*, empty vector or the indicated mutant *sac3* alleles under the endogenous *SAC3* promoter. The *sac3 R256* and *R288* mutants (see D) are labeled in red. Cell density was normalized, and cells were spotted onto plates in 10-fold serial dilutions. Plates were incubated for 2–3 days at the indicated temperatures.

See also Figure S2 and Table S1.

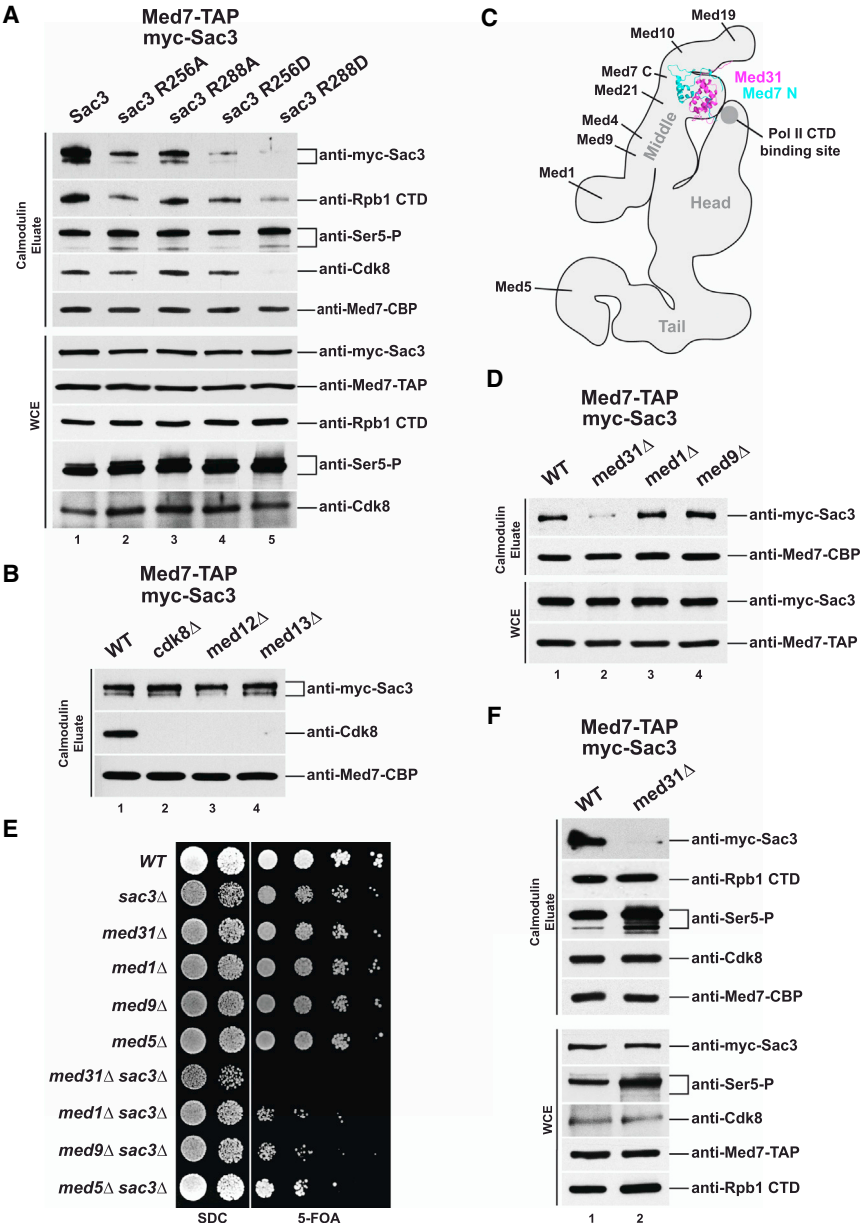

Figure 3. TREX-2 Interaction with Mediator Requires the Sac3 PCI Domain and Med31

(A) TAP-tagged Med7 was purified from *sac3*Δ cells, which were transformed with plasmids carrying N-terminally myc-tagged wild-type or mutant alleles of *SAC3*. Calmodulin eluates and whole cell extracts were immunoblotted with the indicated antibodies. The faster migrating band of myc-Sac3 is a commonly observed degradation product. Med7 immunoblotting was used for normalization. Note that the mutant Sac3 proteins were expressed at similar levels as the wild-type protein.

(B) Med7-TAP purifications from the indicated cells were analyzed by immunoblotting. For Cdk8 WCE levels see Figure 2C.

(C) Mediator cartoon with the crystal structure of Med31/Med7N docked into the prominent protrusion on the "middle" module. Approximate position of the Pol II CTD binding site is marked and additional middle subunits are indicated. All data based on Tsai et al. (2014).

(D) Med7-TAP was purified from the indicated strains, which were transformed with a myc-Sac3 plasmid and analyzed by immunoblotting.

(E) Genetic interaction analysis. Single mutant strains were transformed with an empty vector and the double mutants with a *SAC3* wild-type cover plasmid (URA3). Growth was followed on SDC and on SDC+5-FOA plates to shuffle out the cover plasmid.

(F) Immunoblot analysis of the indicated Med7-TAP strains containing a myc-Sac3 plasmid.

See also Figure S7B.

different degrees as *med13*Δ led to the dissociation of the entire module from Mediator, *med12*Δ dissociated mainly Cdk8 (CycC was not determined) and *cdk8Δ* lacked the kinase (Figure S2E). We found similar, although less pronounced, effects as in *sac3Δ* cells: the amount of Pol II co-purifying with Mediator was reduced, while CTD Ser5 phosphorylation of the residually interacting Pol II was increased (Figure 2C). To substantiate the functional link between TREX-2 and Cdk8 in vivo we employed yeast genetics. Deletion of *CDK8* alone confers a growth defect but is not lethal, implying genetic buffering by other factors. Interestingly, the combination with a *SAC3* deletion caused synthetic lethality (Figure 2D) and this relates to the *SAC3 R288* residue within the PCI domain and the catalytic activity of *CDK8* as shown by a point mutation in the enzyme's active site (Figure 2E). These genetic links are specific to the conserved N-terminal region of the Sac3 PCI domain because a *K467D/K468D* double mutant located in the Sac3 winged helix domain did not exhibit a synthetic growth defect with *cdk8Δ* (Figure 2D). Taken together, our biochemical and genetic data demonstrate a functional synergy between Cdk8 and TREX-2 in vivo and are consistent with their joint regulatory effect on Pol II Ser5 phosphorylation.

TREX-2 Associates with Mediator through the Conserved Sac3 Surface

To find out whether the influence of TREX-2 on Mediator is direct, Mediator was purified from cells expressing N-terminally myc-tagged versions of Sac3 (Figure 3A). Indeed, the TREX-2 core subunit Sac3 could be readily detected in Mediator purifications. Notably, mutation of either Sac3 R256 or R288 resulted in significantly lower amounts of TREX-2 associated with Mediator. This effect was particularly pronounced when the charge of the side-chain was inverted (i.e., R256D and R288D). The *sac3 R288D* mutant, which displayed the weakest affinity toward Mediator

partially recapitulated the deletion of the entire *SAC3* gene with respect to Cdk8 disassembly, Pol II dissociation, and increased Ser5 phosphorylation levels. To investigate whether TREX-2 binds Mediator through the CKM, we tested whether deletions of kinase module subunits would impair TREX-2 binding. However, TREX-2 co-purified efficiently with Mediator even when the module was disrupted (Figure 3B). Thus, TREX-2 regulates association of the CKM with Mediator, yet, without using the CKM as a docking site.

TREX-2 Association with Mediator Requires Med31

The CKM interacts with core Mediator primarily through the middle and "head" module (see Figure 2C) (Tsai et al., 2013). We considered that the TREX-2 PCI domain might interact with Mediator in vicinity of the CKM and initially focused on the elongated Mediator middle module, which extends from Med19 at the tip downward to the Med1 subunit (Figure 3C) (Tsai et al., 2014). As Med4, Med7, Med10, and Med21 deletions are lethal and Med19 deletion destabilizes Mediator (data not shown), we analyzed the co-purification of myc-tagged Sac3 in Mediator purifications deleted for Med1, Med9, and Med31. Notably, TREX-2 association with Mediator was impaired specifically upon loss of the Med31 subunit (Figure 3D). Med31 is one of the most conserved Mediator subunits and required for activated transcription (Koschubs et al., 2009). It interacts with the Med7 N terminus and forms a distinct protrusion on the middle module as seen by cryo-EM (Figure 3C) (Plaschka et al., 2015; Tsai et al., 2014). Significantly, Med31 is located right across a Pol II CTD-interacting region of the head module (Robinson et al., 2012; Tsai et al., 2014). To further explore whether TREX-2 function depends on Med31 in vivo, we tested for potential genetic interactions. In fact, *SAC3* and *MED31* exhibit a synthetic lethal relationship, which involves the conserved *SAC3 R288* residue (Figures 3E and S2F) whereas the other middle module subunits *MED1* and *MED9* or the tail subunit *MED5* showed less pronounced synthetic effects when deleted together with *SAC3*. Given that TREX-2 regulates Ser5 CTD levels, we hypothesized that Med31, being located in vicinity of the Pol II CTD binding site, may act in a similar way. Indeed, deletion of Med31 leads to increased Ser5 CTD phosphorylation levels of the Mediator-bound Pol II, however, without disrupting the Pol II interaction or dissociating Cdk8 (Figure 3F). Taken together, TREX-2 binding to Mediator depends on Med31, which is located in close proximity to the Pol II CTD binding site.

The Med31 Submodule Interaction with TREX-2 Can Be Reconstituted In Vitro

We noticed in our crystal structure, that the Sac3 α1-α2 helix pair, which contains the critical R256 and R288 residues, establishes a dimeric interface with the α1-α2 motif of an adjacent Sac3 molecule (Figures 4A and S2B). A highly similar crystal contact is present in the other TREX-2 PCI structure (PDB: 3t5v), even though this structure was obtained with different protein constructs captured in another crystal packing (Ellisdon et al., 2012). Owing to the conservation of this crystal contact, we hypothesized that the respective interface ($\sim$600 Å^2, a size typically observed for transient interactions) may represent a physiologically relevant, low-affinity protein interaction site of Sac3. To this end, we developed an on-bead binding assay in which stringently purified Mediator was immobilized on IgG beads and incubated with a 5- to 10-fold molar excess of the recombinant TREX-2 PCI domain. TREX-2 binding was then determined by detecting the Thp1-FLAG subunit. Notably, the TREX-2 PCI domain bound to Mediator in a dose-dependent manner and this interaction specifically required the conserved Sac3 R288 residue (Figure 4B), a result that is consistent with our purifications from yeast (Figure 3A). To validate a direct involvement of Med31, we tested binding of the TREX-2 PCI domain to Mediator purified from *med31*Δ cells (note that Mediator stability is not altered) (Koschubs et al., 2009). The recombinant TREX-2 complex showed a substantially reduced affinity toward Mediator that lacked the Med31 subunit (Figure 4C), a result that again mirrors our purifications from cells (Figure 3D). Finally, we tested whether the TREX-2 PCI domain could directly interact with the Med31 submodule. To this end we co-expressed GST-tagged Med31 with an N-terminal fragment of Med7 (aa 1–83) in bacteria and purified the stable heterodimer. Med31 alone is insoluble probably because the Med31/Med7N interface is mainly hydrophobic (Koschubs et al., 2009). We then performed binding assays using TREX-2 PCI domains harboring wild-type Sac3 proteins or charge-inverted mutants of the conserved Sac3 R288 or R256 residues. Notably, we detected a transient complex formation, which was diminished in both mutants, with R288D exhibiting the greatest loss of affinity (Figure 4D). In sum, TREX-2 interacts directly with the Mediator Med31/Med7N submodule in vitro, independently of ongoing transcription and other factors.

The Sac3 PCI Domain Regulates Transcription In Vivo

As Sac3 directly interacts with the Med31 submodule and influences Cdk8 recruitment to Mediator, we analyzed the effects of deleting these three factors on gene expression in vivo. The *GAL1* gene is a paradigm for studies on inducible transcription and gene-NPC targeting. When analyzing Pol II occupancy at *GAL1* after galactose induction by chromatin immunoprecipitation (ChIP), we observed strongly decreased recruitment of Pol II to the promoter and coding region in *sac3*Δ, *med31*Δ, and *cdk8*Δ cells (Figure 5A). Consequently, *GAL1* mRNA levels were decreased in all mutants (Figure S3A). The downregulation of transcription was also seen for the *sac3 R288D* mutation, underscoring the critical function of this residue for highly inducible transcription. To identify the target genes of TREX-2 on a genome-wide scale we performed chromatin immunoprecipitation-exonuclease (ChIP-exo) assays, a high-resolution method that combines chromatin immunoprecipitation (ChIP) with lambda exonuclease digestion followed by high-throughput sequencing (Rhee and Pugh, 2011). Despite extensive efforts we could not detect specific enrichment of the TREX-2 subunit Thp1-TAP anywhere on the genome (Figure S4A). This contrasts with a recent report that describes genome-wide enrichment of Thp1 at highly transcribed genes using ChIP-chip (Santos-Pereira et al., 2014). When we analyze the putative TREX-2 target genes identified in that study, we find indistinguishable ChIP-exo patterns between Thp1-TAP and the mock control (untagged Thp1) in replicate experiments (Figure S4B). This is in line with

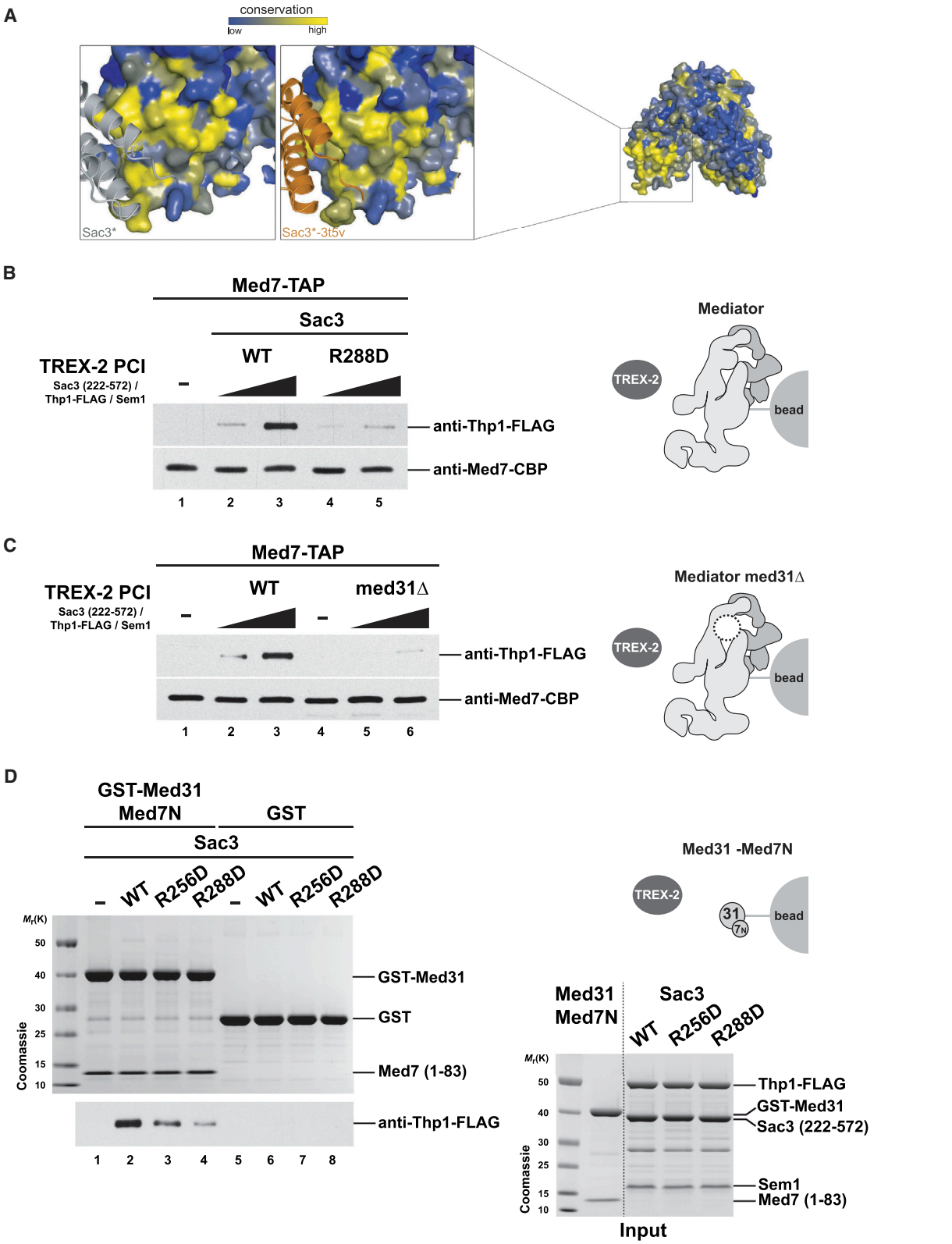

(legend on next page)

two earlier studies (Park et al., 2013; Teytelman et al., 2013) that demonstrated artifactual enrichment of ChIP signals at highly transcribed genes, which we confirm. We thus suggest caution when interpreting TREX-2 enrichment at highly expressed genes. Our results do not rule out the presence of TREX-2 at active genes, but this remains to be demonstrated. Given the physical interaction of TREX-2 with Mediator, we suggest that Thp1 may not be within crosslinkable distance to DNA. Alternatively, TREX-2 may undergo a similarly rapid Pol II Ser5-P-dependent dissociation at yeast promoters as Mediator, a feature that complicates Mediator detection (Jeronimo and Robert, 2014).

Expression Profiling Reveals a Specific Pathway Co-regulated by TREX-2 and Med31

To examine the genome-wide influence of TREX-2 and Mediator in vivo, we performed gene expression profiling by RNA sequencing (RNA-seq) with *sac3*Δ and *cdk8*Δ strains and the *sac3 R288D* mutant. These datasets were compared to the *med31*Δ transcriptome (Koschubs et al., 2009) by hierarchical clustering of deletion signatures using a stringent 2-fold cutoff and a false discovery rate of $p < 0.05$ (Figure 5B). Compared to wild-type, the expression profile of *sac3 R288D* and *sac3*Δ cells are similar as reflected by their Pearson's correlation coefficient (Figures 5C and S3B). This confirms the functional importance of the PCI domain surface implicated in Mediator binding. Differences to the *sac3*Δ transcriptome may hint at additional functions of other TREX-2 subunits. Correlation analyses did not reveal a broad overlap between *sac3*Δ and the *med31*Δ or *cdk8*Δ gene expression profiles consistent with TREX-2 and Mediator being separate entities. Similarly, the *med31*Δ and *cdk8*Δ profiles were weakly correlated (Figures 5C, 5D, and S3B). The latter result is surprising but agrees with previous expression data (van de Peppel et al., 2005) and shows that despite residing in the same complex, different Mediator modules regulate distinct target genes with some modules even antagonizing each other. To identify biological functions common to *SAC3* and *MED31*, we performed gene ontology (GO) analyses of significantly altered mRNAs. Amid the downregulated genes, sulfur amino acid biosynthesis was the highest scoring GO term. Interestingly, genes involved in sulfate/methionine metabolism are also significantly overrepresented in the *med31*Δ profile (Koschubs et al., 2009) (Figures 5E and S3D; Table S5). qPCR measurements of ten target genes in this pathway verified their general downregulation in *sac3*Δ and *med31*Δ cells, while these genes were mostly upregulated in *cdk8*Δ cells (Figure S3E). Significantly, a phenotypic analysis confirmed that in the absence of methionine, an end product of the pathway, *med31*Δ, *sac3*Δ, or *sac3 R288D* cells exhibited robust growth defects (Figure 5F), thus validating the transcriptome results. Pervasive low-magnitude transcriptome changes in other co-regulated genes may also be biologically relevant but this remains to be analyzed by profiling multiple growth conditions. Here, we were able to pinpoint a specific cellular pathway that illustrates the functional convergence of *MED31* and *SAC3* on constitutive gene expression.

The Sac3 PCI Surface and Mediator Are Required for Gene-NPC Targeting

Given the role of TREX-2 in promoting the targeting of the highly inducible *GAL1* gene to NPCs ("gene gating") (Cabal et al., 2006), we asked whether the functional interface between TREX-2 and Mediator could be involved. To this end, we monitored the location of *GAL1* relative to the nuclear periphery in transcriptionally repressed and activated conditions. Notably, as for *sac3*Δ cells (Cabal et al., 2006), the *sac3 R288D* mutation interferes with the repositioning of the activated *GAL1* gene to NPCs (Figure 6). Impaired NPC targeting was seen in *med31*Δ cells, but not in *cdk8*Δ cells (Figure 6), in which *GAL1* repositioning to the periphery occurred normally despite reduced *GAL1* mRNA levels (Figure S3A). To test another "gated" model gene, we analyzed the subtelomeric *HXK1*, which becomes activated and targeted to NPCs by removing glucose (e.g., growth in galactose) (Taddei et al., 2006). Promoter activation did not significantly increase *HXK1* relocalization to the periphery in *sac3*Δ cells (Figure S5A; see Figure S5B for expression levels). In contrast to *GAL1* regulation, *HXK1* repositioning was impaired by the deletion of both *MED31* and *CDK8* (Figure S5A). The gene-NPC targeting defects in these mutants are not caused by indirect effects on the NPC anchor element of TREX-2 (Figure 1A), because Sac3 remained properly attached to NPCs in *med31*Δ and *cdk8*Δ cells (Figure S6A; see Figure S6B for phenotypes). In sum, Mediator and TREX-2 are both required for NPC-targeting of the highly inducible *GAL1* and *HXK1* genes. Differences in Cdk8-dependancy likely reflect how Mediator "interprets" a gene-specific context of transcription factors, illustrated by the fact that Hxk2, a *HXK1*-specific transcriptional repressor, binds to Mediator via Med8 (de la Cera et al., 2002), whereas the *GAL1* transcription activator Gal4 interacts with Med17 and Cdk8 (Traven et al., 2006).

Figure 4. TREX-2 Interacts with the Med31/Med7N Submodule In Vitro

(A) Crystal contact observed in the crystal lattice of two different TREX-2 PCI domain complexes. Helices α1, α2, and α4 of Sac3 compose a highly conserved surface region that is key to interact with molecular neighbors (*) in the present crystal form (gray) and in the previously reported crystal structure (PDB: 3t5v, orange). See also Figure S2B.

(B) In vitro reconstitution of the interaction between Mediator and the TREX-2 PCI domain. Mediator was purified by IgG-Protein A affinity-purification from yeast and incubated on beads with recombinant wild-type or mutant sac3 R288D TREX-2 PCI domain complexes containing Flag-tagged Thp1 (see D for input) in an ~1:5 and 1:10 molar ratio of Mediator:TREX-2. Following washing and TEV protease elution, samples were analyzed by immunoblotting. Med7 was used for normalization.

(C) Same set-up as in (B) except that wild-type Mediator was compared to Mediator purified from *med31*Δ cells.

(D) In vitro binding assay using the recombinant GST-Med31/Med7N heterodimer or GST as negative control. Proteins were immobilized on GSH beads and incubated with the recombinant wild-type or mutant TREX-2 PCI domain complexes. Following elution, Thp1-FLAG was detected by immunoblotting. Inputs are shown on the right.

See also Figure S7B.

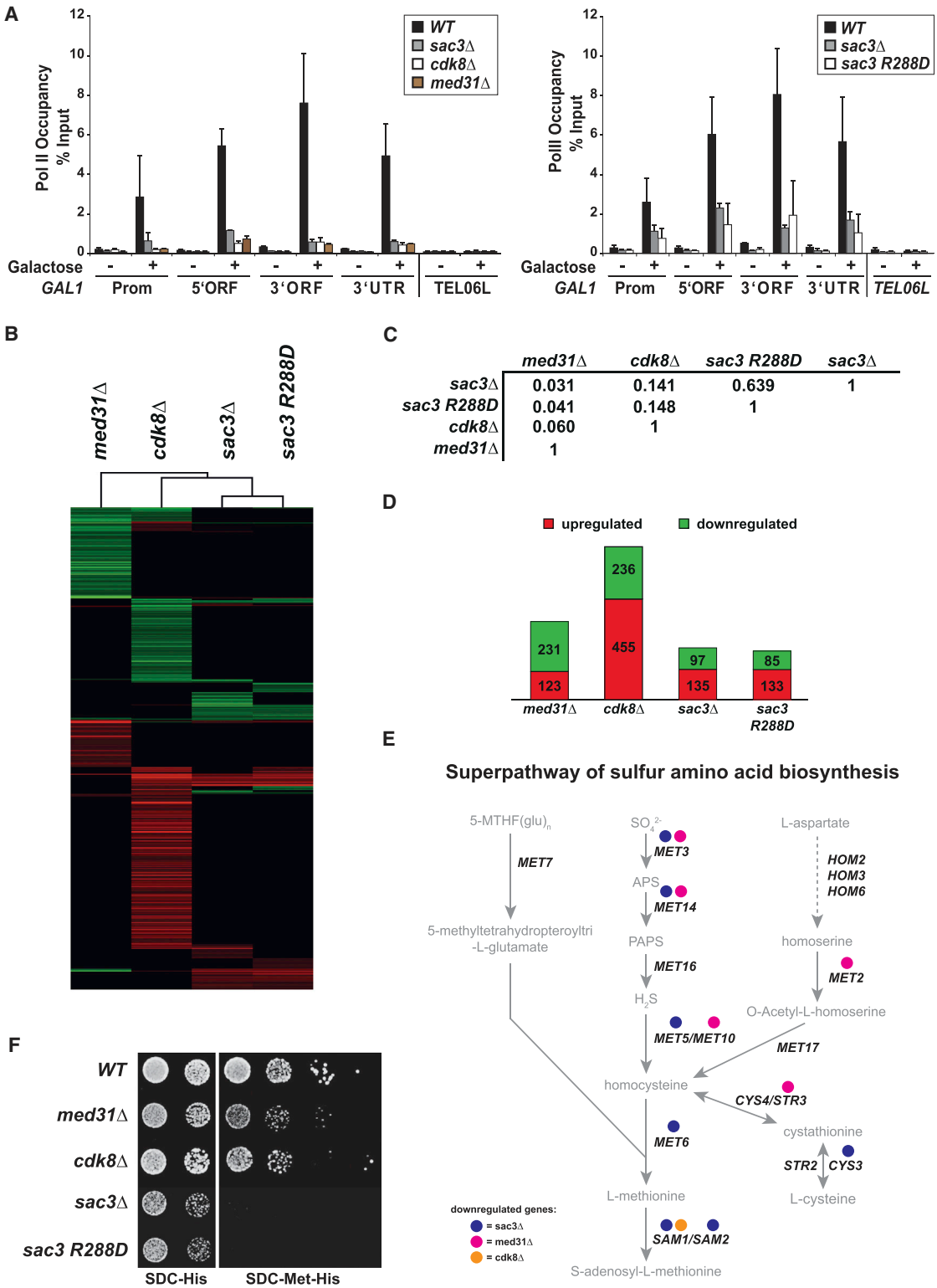

Figure 5. The Sac3 PCI Domain Is Required for Transcription of Specific Genes In Vivo

(A) Pol II occupancy at the *GAL1* promoter (Prom), 5′ORF, 3′ORF, and 3′UTR region was analyzed by ChIP in *WT* and mutant cells. Cells were either grown in raffinose or induced with 2% galactose for 120 min. Pol II occupancy at telomere 06L is shown as a negative control. Error bars represent SD of three independent experiments. qPCR primers are listed in Table S2.

(legend continued on next page)

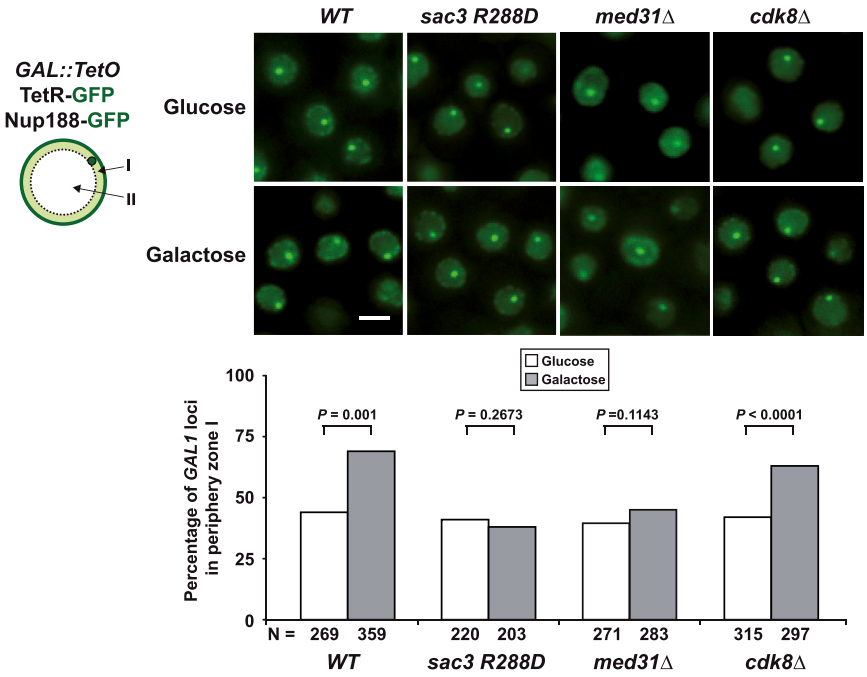

Figure 6. The Sac3 PCI Domain and Med31 Are Required for Gene-NPC Targeting

GAL1-NPC targeting assay. The *GAL1* locus is tagged with TetO repeats, which are labeled with TetR-GFP, the nuclear envelope is labeled with Nup188-GFP. *sac3*Δ cells were transformed with plasmids carrying either *SAC3* wild-type, or the *sac3 R288D* allele, *cdk8*Δ cells contained an empty plasmid. For each strain, examples are shown both in glucose and galactose (scale bar, 2 μm). After z stack acquisition, the position of the labeled *GAL1* locus was determined in those cells where the brightest *GAL1* signal and the largest nuclear diameter were in the same z section. The bar graph shows the proportion of *GAL* loci found in the peripheral volume (zone I). Comparisons of *GAL1* distributions for each strain and growth condition were performed using the one-tailed Fisher's exact test. The p value is indicated for each test and N, the total number of cells analyzed, is shown at the bottom of the bars. Results were reproduced in an independent experiment: *wild-type*: n = 201 (glucose) and 230 (galactose), $p < 0.0001$; *sac3 R288D*: n = 190 (glucose) and 198 (galactose), p = 0,3112; *cdk8*Δ: n = 252 (glucose) and 214 (galactose), $p < 0,0001$. For analysis of a control gene not affected by TREX-2 see Figure S5C. See also Figure S6.

The Conserved TREX-2 Surface Affects Both Transcription and mRNA Export

As TREX-2 deletion causes an mRNA export defect (Fischer et al., 2002; Gallardo et al., 2003), we explored whether the conserved Sac3 PCI domain surface is involved. To this end, we assessed cellular mRNA distribution using in situ hybridization with probes against the mRNA poly(A) tail (Figure S7A). Compared to wild-type cells, which contain abundant mRNA in the cytoplasm, both the *sac3 R256D* and *R288D* mutant exhibited a nuclear retention of mRNA indicative of an mRNA processing/export defect. In contrast, *MED31* and *CDK8* deletion caused no major mRNA export defect. Hence, the interaction between the Sac3 PCI and the Med31 submodule is not absolutely required for mRNA export, whereas the conserved Sac3 PCI domain surface is. The functions of Sac3 and Med31, although interdependent, are mechanistically separable. This suggests a mechanism in which TREX-2 promotes mRNP formation/export through the conserved Sac3 PCI domain surface, which is co-opted for transcriptional regulation via Mediator. In analogy to the multiple protein-RNA handover reactions that occur during mRNP biogenesis, TREX-2 may sequentially interact with Mediator and mRNP factors downstream of transcription initiation.

DISCUSSION

In this study, we describe a direct link between the TREX-2 complex and Mediator, which is key to understanding how NPC-associated adaptors modulate gene expression (Figure 7). We find that the TREX-2 complex (1) interacts with the Mediator Med31 submodule via the Sac3 PCI domain, (2) regulates Mediator association with the Cdk8 kinase, (3) impacts on Pol II CTD Ser5 phosphorylation, and (4) employs a similar, conserved Sac3 PCI domain surface to promote transcription and mRNA export. This sheds light on the biological function of TREX-2 and opens new avenues for reconstituting the interface between nuclear pores, adaptor proteins, and the core transcription machinery.

Interaction Mode of TREX-2 and Mediator

The PCI domain surface appears structurally "simple," but its function is intricate. To infer how TREX-2 regulates Mediator, it is instructive to consider the location of its docking site. The Med31/Med7N submodule lies in vicinity of two Mediator landmarks: (1) the Pol II CTD binding site on the head, and (2) a CKM binding site on the middle module (Figure S7B). Med31 is connected to the elongated middle module via an unstructured linker in Med7, which suggests conformational mobility at the

(B) Cluster diagram of genes with significantly altered mRNA levels (>2.0-fold) in Mediator or TREX-2 mutant cells. Changes in mRNA levels compared to the wild-type strain are depicted in red (up), green (down), or black (no change).
(C) Pearson's correlation matrix for expression profiles of TREX-2 and Mediator mutant strains as indicated (FC > 2.0 and FDR < 0.05).
(D) Number of significantly altered genes of all investigated strains. See also Figure S3C.
(E) Schematic view of sulfur amino acid biosynthesis superpathway. Genes with reduced expression in *sac3*Δ, *med31*Δ, or *cdk8*Δ cells are indicated.
(F) Growth analysis of *WT*, *cdk8*Δ, *med31*Δ, and *sac3* mutant strains on medium with and without methionine. All BY4741 strains were transformed with a pRS411 (MET) plasmid to allow growth on methionine-deficient media.
See also Figures S4 and S7A and Table S5.

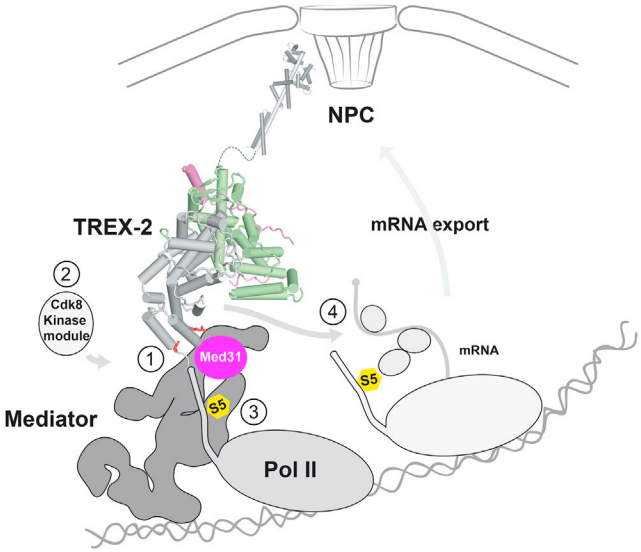

Figure 7. The Sac3 PCI Domain Promotes Transcription and mRNA Export

Mechanism for a relay between TREX-2, Mediator, and Pol II. Model depicts the putative overall topology of TREX-2 and its interaction with Mediator. (1) Docking to Mediator involves the conserved pair of Sac3 R256/R288 residues (red sticks) and the Med31 submodule (magenta). (2) TREX-2 regulates Cdk8 kinase module association. (3) TREX-2, Cdk8, and Med31 impact on RNA Pol II CTD Ser5 phosphorylation (S5; yellow). (4) TREX-2 also influences mRNA export via the PCI surface centered around the Sac3 R256/R288 residues. Other mRNA adaptor/export proteins are depicted as circles. Transition between Pol II initiation and early elongation is shown. TREX-2 attaches to the NPC basket through an NPC anchor domain comprising a 12.5 nm long Sac3 helix, two Sus1 molecules and Cdc31 (all in gray, PDB: 3fwc).

interface between the middle and head modules (Figure S7B). Accordingly, Med31 deletion results in substantial rearrangements of Mediator architecture (Tsai et al., 2014). Viewed in this context, the docking of the Sac3 PCI domain onto the Med31/Med7N submodule could locally alter Mediator conformation and thereby regulate interactions with Pol II. The same principle probably extends to the Cdk8 kinase module (CKM), which interacts with core Mediator mainly through a contact between the middle module subunit Med19 and through a region of the Mediator head. Yeast Med19 is located at the tip of the flexible Med7/Med21 subcomplex that in turn anchors Med31 (Figure S7B). Hence, the close proximity of relevant binding sites could explain the dual effect that TREX-2 exerts on Pol II and the CKM.

A Network of Factors Modulate Ser5 Phosphorylation of the Pol II CTD

An intriguing finding of this study is that Sac3, Med31, and Cdk8 are all required for normal Ser5-P levels, a CTD mark that defines transcription initiation. Mediator is thought to orient TFIIH with respect to the Pol II CTD (Plaschka et al., 2015), thereby promoting CTD phosphorylation and Pol II promoter escape (Jeronimo and Robert, 2014). Given the proximity of Med31 to the CTD, the docking of TREX-2 could impact on how Mediator topologically "presents" the CTD to the TFIIH kinase Kin28 for phosphorylation, affect Kin28 enzymatic activity itself or impinge on an inhibitory cross-talk between Cdk8 and Kin28, which was reported for the human proteins (Akoulitchev et al., 2000). Our data suggest that when Med31 is lacking and TREX-2 is unable to contact Mediator, Cdk8 cannot properly exert its influence on TFIIH. We further noticed that TREX-2 has more pronounced effects on global Ser5-P levels than Cdk8 or Med31. This may be explained by Sac3 affecting both Cdk8 and Med31 function. The dissociation of Pol II from Mediator seen in *sac3*Δ cells could then result from the strongly hyperphosphorylated Pol II CTD. This view is consistent with reports implicating Ser5 phosphorylation in the dissociation of Mediator and Pol II during transcription initiation (Jeronimo and Robert, 2014; Søgaard and Svejstrup, 2007; Wong et al., 2014). Hence, we propose that TREX-2 in conjunction with other factors impinges on transcription initiation by setting the right balance of Pol II CTD phosphorylation. While further work is required to clarify the structural details, our data strongly suggests that TREX-2 binds Mediator in a strategic position to influence critical protein transactions.

TREX-2 Function in the Promoter Context

A long-standing question in NPC biology is how the targeting of genes to the nuclear pore alters their transcription. Earlier work reported a transient association between the co-activator SAGA and TREX-2 (Köhler et al., 2008; Rodríguez-Navarro et al., 2004). While SAGA and TREX-2 by themselves are critical for gene-NPC targeting of *GAL1* (Cabal et al., 2006), it remained unclear whether the interaction between SAGA and TREX-2 is direct and how Pol II regulation is achieved. Our present work goes beyond previous studies by identifying a direct cross-talk between TREX-2, Mediator, and Pol II, which influences both inducible and constitutive gene expression. This supports the notion that TREX-2 interacts with promoter-bound factors; yet, its mode of regulating gene expression is directly linked to Mediator. Based upon existing models on transcription initiation it is expected that Mediator and SAGA co-occupy numerous yeast promoters (Venters et al., 2011). Possibly, TREX-2 can contact both SAGA and Mediator given that SAGA modulates the TREX-2 C-terminal domain (Köhler et al., 2008), whereas Mediator interacts with the PCI domain (Figure 7). Yeast TREX-2 localizes mainly to the NPC basket, however, this interaction is regulated (Fischer et al., 2004; Köhler et al., 2008). Conceivably, a fraction of TREX-2 can shuttle between NPCs and the nuclear interior, thereby expanding its operating range. By contacting Mediator, TREX-2 utilizes Mediator's known ability to integrate external signals like transcription factors and co-activators and directly communicate them to the general Pol II machinery. For NPC-targeted highly inducible genes, Mediator may "sense" the presence of the NPC through TREX-2 and in doing so optimize transcriptional outputs as a way of responding to the gene's location.

EXPERIMENTAL PROCEDURES

Yeast Strains and Plasmids

Yeast strains and plasmids are listed in Tables S3 and S4, respectively. Microbiological techniques followed standard procedures.

Affinity Purifications and Immunoblotting

Tandem affinity purifications from yeast were performed according to (Köhler et al., 2008), for details of mass spectrometry see Table S6. Cells were grown in YPD or when transformed with plasmids in selective SDC drop-out medium. Antibodies are listed in the Supplemental Information.

Protein Overexpression, Purification, and Crystallization

The *S. cerevisiae* gene fragments of *6HIS-TEV-SAC3(222-572)*, *THP1(170-455)*, and full-length *SEM1* were co-expressed in BL21-CodonPlus(DE3)-RIL *Escherichia coli* cells. Following Ni-NTA chromatography, TEV cleavage and size exclusion, proteins were concentrated to 10–15 mg/ml in 10 mM $NaP0_4$ (pH 7.5), 150 mM NaCl. After adding TCEP (1 mM final), crystals were grown by sitting-drop vapor diffusion in 0.5 M $LiSO_4$, 10% PEG 8.000 at 19°C. Upon incubation in the reservoir solution (30% glycerol as cryoprotectant), crystals were flash frozen in liquid N_2.

Diffraction Data Collection, Processing, and Structure Solution

Diffraction data were collected at the Swiss Light Source beamline X06SA, integrated with XDS and scaled with SCALA (Evans, 2006; Kabsch, 2010). Molecular replacement was performed using the previously solved Sac3/Thp1/Sem1 structure (PDB: 3t5v) from which Thp1 residues 2–169 were omitted. See Supplemental Experimental Procedures and Table S1 for details. Coordinates have been deposited to the Protein Data Bank (PDB: 4trq).

Gene Localization, Expression, and FISH Experiments

Imaging was performed on a DeltaVision Elite microscope (GE Healthcare). Localization of poly(A)$^+$ RNA by in situ hybridization was performed using a Cy3 end-labeled oligo. See Supplemental Experimental Procedures for details.

Chromatin Immunoprecipitation

Pol II occupancy on *GAL1* was determined after induction for 2 hr. The ChIP method contains minor modifications of a published protocol (see Supplemental Experimental Procedures and Table S2).

In Vitro Binding Assays

Mediator complexes were purified via Med7-TAP on IgG beads and washed with 150 ml standard TAP buffer. Recombinant TREX-2 was added to the IgG-bound Mediator complex, co-incubated for 1 hr, washed with 25 ml buffer and eluted by TEV cleavage. GST-Med7N and Med31 were bacterially co-expressed, immobilized on glutathione (GSH) beads, and after incubation with recombinant TREX-2, washed and eluted with GSH.

ACCESSION NUMBERS

The accession number for the coordinates reported in this paper is PDB: 4trq.

SUPPLEMENTAL INFORMATION

Supplemental Information includes Supplemental Experimental Procedures, seven figures, and six tables and can be found with this article online at http://dx.doi.org/10.1016/j.cell.2015.07.059.

AUTHOR CONTRIBUTIONS

M.S. purified proteins for crystallization. D.H. crystallized the complex and solved the structure with T.C. M.S. performed in vitro biochemistry, TAP purifications, FISH experiments, yeast genetics, and with A.K., gene localization studies. T.S. performed TAP purifications, mRNA quantification, and ChIP. V.V., R.R., and B.F.P. carried out ChIP-exo. S.A. performed mutational analyses. A.K. designed the study and wrote the paper.

ACKNOWLEDGMENTS

We thank J. Cibulka and K. Lipp for assistance, the CSF NGS unit for RNA-seq, and S. Juntilla (CSF Biocomp) for bioinformatic analyses. We acknowledge R. Young, Y. Takagi, C. Dargemont, and D. Bentley for antibodies, S. Tan for the pST44 vector and G. Warren and J. Brennecke for comments on the manuscript. A. Köhler is funded by an ERC grant (281354; NPC GENEXPRESS) and a START grant from the Austrian Science Fund (FWF; Y557-B11). The IMP is funded by Boehringer Ingelheim. B.F.P. is funded by NIH grant GM059055 and has a financial interest in Peconic, LLC, which utilizes ChIP-exo and could potentially benefit from the outcomes of this research.

Received: June 18, 2014
Revised: May 5, 2015
Accepted: July 6, 2015
Published: August 27, 2015

REFERENCES

Ahmed, S., Brickner, D.G., Light, W.H., Cajigas, I., McDonough, M., Froyshteter, A.B., Volpe, T., and Brickner, J.H. (2010). DNA zip codes control an ancient mechanism for gene targeting to the nuclear periphery. Nat. Cell Biol. *12*, 111–118.

Akoulitchev, S., Chuikov, S., and Reinberg, D. (2000). TFIIH is negatively regulated by cdk8-containing mediator complexes. Nature *407*, 102–106.

Bermejo, R., Capra, T., Jossen, R., Colosio, A., Frattini, C., Carotenuto, W., Cocito, A., Doksani, Y., Klein, H., Gómez-González, B., et al. (2011). The replication checkpoint protects fork stability by releasing transcribed genes from nuclear pores. Cell *146*, 233–246.

Borggrefe, T., Davis, R., Erdjument-Bromage, H., Tempst, P., and Kornberg, R.D. (2002). A complex of the Srb8, -9, -10, and -11 transcriptional regulatory proteins from yeast. J. Biol. Chem. *277*, 44202–44207.

Cabal, G.G., Genovesio, A., Rodriguez-Navarro, S., Zimmer, C., Gadal, O., Lesne, A., Buc, H., Feuerbach-Fournier, F., Olivo-Marin, J.C., Hurt, E.C., and Nehrbass, U. (2006). SAGA interacting factors confine sub-diffusion of transcribed genes to the nuclear envelope. Nature *441*, 770–773.

de la Cera, T., Herrero, P., Moreno-Herrero, F., Chaves, R.S., and Moreno, F. (2002). Mediator factor Med8p interacts with the hexokinase 2: implication in the glucose signalling pathway of Saccharomyces cerevisiae. J. Mol. Biol. *319*, 703–714.

Ellisdon, A.M., Dimitrova, L., Hurt, E., and Stewart, M. (2012). Structural basis for the assembly and nucleic acid binding of the TREX-2 transcription-export complex. Nat. Struct. Mol. Biol. *19*, 328–336.

Evans, P. (2006). Scaling and assessment of data quality. Acta Crystallogr. D Biol. Crystallogr. *62*, 72–82.

Fischer, T., Strässer, K., Rácz, A., Rodriguez-Navarro, S., Oppizzi, M., Ihrig, P., Lechner, J., and Hurt, E. (2002). The mRNA export machinery requires the novel Sac3p-Thp1p complex to dock at the nucleoplasmic entrance of the nuclear pores. EMBO J. *21*, 5843–5852.

Fischer, T., Rodríguez-Navarro, S., Pereira, G., Rácz, A., Schiebel, E., and Hurt, E. (2004). Yeast centrin Cdc31 is linked to the nuclear mRNA export machinery. Nat. Cell Biol. *6*, 840–848.

Flanagan, P.M., Kelleher, R.J., 3rd, Sayre, M.H., Tschochner, H., and Kornberg, R.D. (1991). A mediator required for activation of RNA polymerase II transcription in vitro. Nature *350*, 436–438.

Gallardo, M., Luna, R., Erdjument-Bromage, H., Tempst, P., and Aguilera, A. (2003). Nab2p and the Thp1p-Sac3p complex functionally interact at the interface between transcription and mRNA metabolism. J. Biol. Chem. *278*, 24225–24232.

González-Aguilera, C., Tous, C., Gómez-González, B., Huertas, P., Luna, R., and Aguilera, A. (2008). The THP1-SAC3-SUS1-CDC31 complex works in transcription elongation-mRNA export preventing RNA-mediated genome instability. Mol. Biol. Cell *19*, 4310–4318.

Ibarra, A., and Hetzer, M.W. (2015). Nuclear pore proteins and the control of genome functions. Genes Dev. *29*, 337–349.

Jeronimo, C., and Robert, F. (2014). Kin28 regulates the transient association of Mediator with core promoters. Nat. Struct. Mol. Biol. *21*, 449–455.

Kabsch, W. (2010). XDS. Acta Crystallogr. D Biol. Crystallogr. *66*, 125–132.

Köhler, A., Schneider, M., Cabal, G.G., Nehrbass, U., and Hurt, E. (2008). Yeast Ataxin-7 links histone deubiquitination with gene gating and mRNA export. Nat. Cell Biol. *10*, 707–715.

Koschubs, T., Seizl, M., Larivière, L., Kurth, F., Baumli, S., Martin, D.E., and Cramer, P. (2009). Identification, structure, and functional requirement of the Mediator submodule Med7N/31. EMBO J. *28*, 69–80.

Liao, S.M., Zhang, J., Jeffery, D.A., Koleske, A.J., Thompson, C.M., Chao, D.M., Viljoen, M., van Vuuren, H.J., and Young, R.A. (1995). A kinase-cyclin pair in the RNA polymerase II holoenzyme. Nature *374*, 193–196.

Liu, Y., Kung, C., Fishburn, J., Ansari, A.Z., Shokat, K.M., and Hahn, S. (2004). Two cyclin-dependent kinases promote RNA polymerase II transcription and formation of the scaffold complex. Mol. Cell. Biol. *24*, 1721–1735.

Park, D., Lee, Y., Bhupindersingh, G., and Iyer, V.R. (2013). Widespread misinterpretable ChIP-seq bias in yeast. PLoS ONE *8*, e83506.

Pick, E., Hofmann, K., and Glickman, M.H. (2009). PCI complexes: Beyond the proteasome, CSN, and eIF3 Troika. Mol. Cell *35*, 260–264.

Plaschka, C., Larivière, L., Wenzeck, L., Seizl, M., Hemann, M., Tegunov, D., Petrotchenko, E.V., Borchers, C.H., Baumeister, W., Herzog, F., et al. (2015). Architecture of the RNA polymerase II-Mediator core initiation complex. Nature *518*, 376–380.

Poss, Z.C., Ebmeier, C.C., and Taatjes, D.J. (2013). The Mediator complex and transcription regulation. Crit. Rev. Biochem. Mol. Biol. *48*, 575–608.

Rhee, H.S., and Pugh, B.F. (2011). Comprehensive genome-wide protein-DNA interactions detected at single-nucleotide resolution. Cell *147*, 1408–1419.

Robinson, P.J., Bushnell, D.A., Trnka, M.J., Burlingame, A.L., and Kornberg, R.D. (2012). Structure of the mediator head module bound to the carboxy-terminal domain of RNA polymerase II. Proc. Natl. Acad. Sci. USA *109*, 17931–17935.

Rodríguez-Navarro, S., Fischer, T., Luo, M.J., Antúnez, O., Brettschneider, S., Lechner, J., Pérez-Ortín, J.E., Reed, R., and Hurt, E. (2004). Sus1, a functional component of the SAGA histone acetylase complex and the nuclear pore-associated mRNA export machinery. Cell *116*, 75–86.

Rougemaille, M., Dieppois, G., Kisseleva-Romanova, E., Gudipati, R.K., Lemoine, S., Blugeon, C., Boulay, J., Jensen, T.H., Stutz, F., Devaux, F., and Libri, D. (2008). THO/Sub2p functions to coordinate 3′-end processing with gene-nuclear pore association. Cell *135*, 308–321.

Santos-Pereira, J.M., García-Rubio, M.L., González-Aguilera, C., Luna, R., and Aguilera, A. (2014). A genome-wide function of THSC/TREX-2 at active genes prevents transcription-replication collisions. Nucleic Acids Res. *42*, 12000–12014.

Søgaard, T.M., and Svejstrup, J.Q. (2007). Hyperphosphorylation of the C-terminal repeat domain of RNA polymerase II facilitates dissociation of its complex with mediator. J. Biol. Chem. *282*, 14113–14120.

Taddei, A., Van Houwe, G., Hediger, F., Kalck, V., Cubizolles, F., Schober, H., and Gasser, S.M. (2006). Nuclear pore association confers optimal expression levels for an inducible yeast gene. Nature *441*, 774–778.

Texari, L., Dieppois, G., Vinciguerra, P., Contreras, M.P., Groner, A., Letourneau, A., and Stutz, F. (2013). The nuclear pore regulates GAL1 gene transcription by controlling the localization of the SUMO protease Ulp1. Mol. Cell *51*, 807–818.

Teytelman, L., Thurtle, D.M., Rine, J., and van Oudenaarden, A. (2013). Highly expressed loci are vulnerable to misleading ChIP localization of multiple unrelated proteins. Proc. Natl. Acad. Sci. USA *110*, 18602–18607.

Thompson, C.M., Koleske, A.J., Chao, D.M., and Young, R.A. (1993). A multisubunit complex associated with the RNA polymerase II CTD and TATA-binding protein in yeast. Cell *73*, 1361–1375.

Traven, A., Jelicic, B., and Sopta, M. (2006). Yeast Gal4: a transcriptional paradigm revisited. EMBO Rep. *7*, 496–499.

Tsai, K.L., Sato, S., Tomomori-Sato, C., Conaway, R.C., Conaway, J.W., and Asturias, F.J. (2013). A conserved Mediator-CDK8 kinase module association regulates Mediator-RNA polymerase II interaction. Nat. Struct. Mol. Biol. *20*, 611–619.

Tsai, K.L., Tomomori-Sato, C., Sato, S., Conaway, R.C., Conaway, J.W., and Asturias, F.J. (2014). Subunit architecture and functional modular rearrangements of the transcriptional mediator complex. Cell *157*, 1430–1444.

van de Peppel, J., Kettelarij, N., van Bakel, H., Kockelkorn, T.T., van Leenen, D., and Holstege, F.C. (2005). Mediator expression profiling epistasis reveals a signal transduction pathway with antagonistic submodules and highly specific downstream targets. Mol. Cell *19*, 511–522.

Venters, B.J., Wachi, S., Mavrich, T.N., Andersen, B.E., Jena, P., Sinnamon, A.J., Jain, P., Rolleri, N.S., Jiang, C., Hemeryck-Walsh, C., and Pugh, B.F. (2011). A comprehensive genomic binding map of gene and chromatin regulatory proteins in Saccharomyces. Mol. Cell *41*, 480–492.

Wong, K.H., Jin, Y., and Struhl, K. (2014). TFIIH phosphorylation of the Pol II CTD stimulates mediator dissociation from the preinitiation complex and promoter escape. Mol. Cell *54*, 601–612.

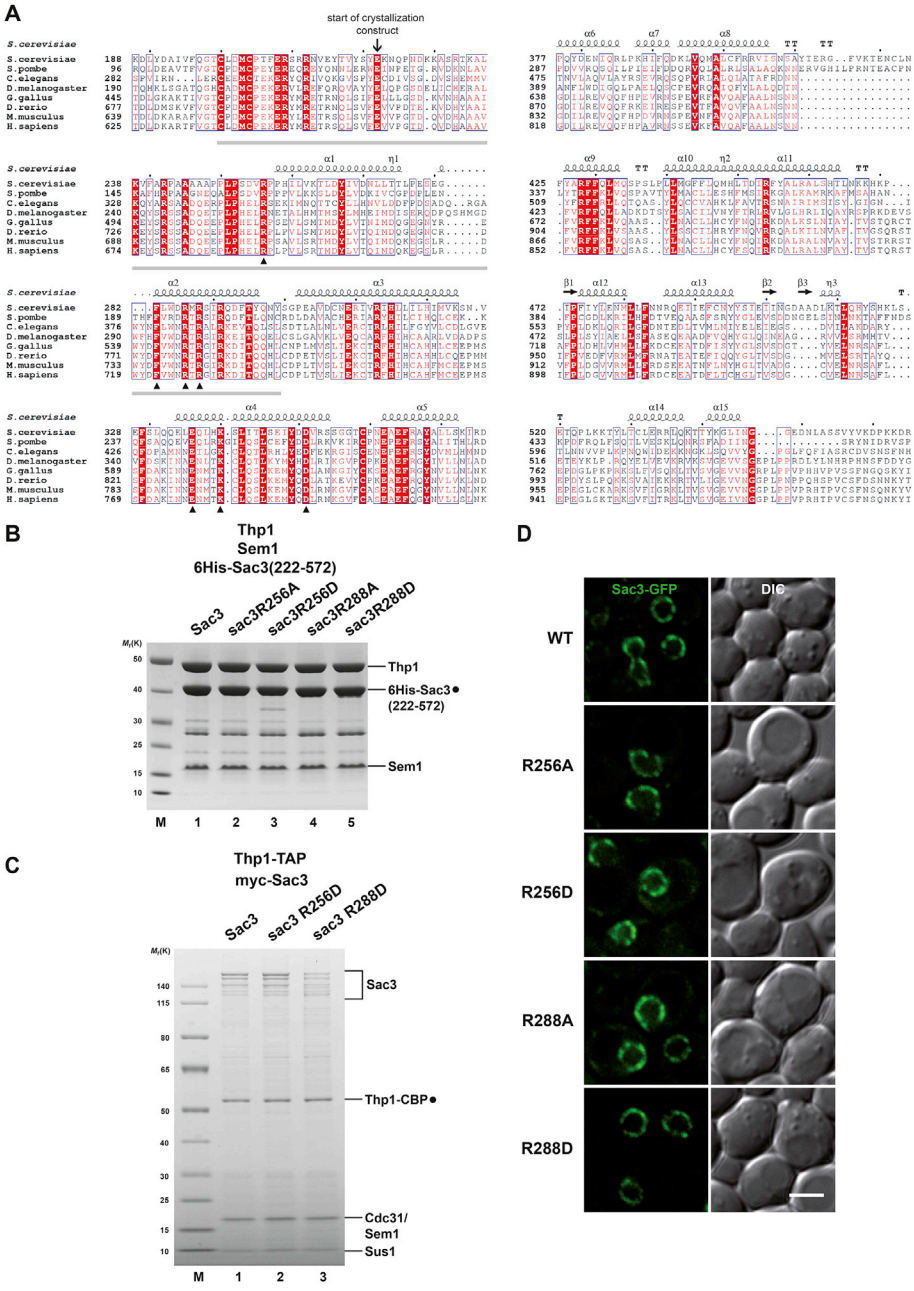

Figure S1. Sac3 Sequence Analysis and Characterization of Sac3 Mutants, Related to Figure 1

(A) Sequence alignment of Sac3 proteins from *S. cerevisiae*, *S. pombe*, *C. elegans*, *D. melanogaster*, *G. gallus*, *D. rerio*, *M. musculus*, and *H. sapiens*. Conserved residues are highlighted in boxes. Strictly conserved residues have a red background. Filled triangles mark strictly conserved residues located within clusters A and B of the Sac3 helical domain. Open triangles label residues Lys467 and Lys468, which are also shown in Figure S2A. Solid gray bar indicates sequence that defines the Sac3 PCI domain as 'atypical' compared to conventional PCI domain variants (Pick et al., 2009).

(B) SDS-PAGE analysis of 6His-Sac3 wild-type and mutant PCI domain complexes after polycistronic expression in *E. coli*, Ni-NTA affinity purification and size-exclusion chromatography on a Superdex 200 column.

(C) TREX-2 purification from yeast cells. Thp1-TAP sac3Δ strains were transformed with the indicated N-terminally myc-tagged *SAC3* plasmids (endogenous promoter) and subject to tandem-affinity purification. The full-length Sac3 protein typically shows variable signs of degradation. Sus1 and Cdc31 bind to the C-terminal domain of TREX-2 (see Figure 1A) and their stoichiometry with respect to Thp1 is a good proxy of overall complex integrity.

(D) Localization of N-terminally GFP-tagged Sac3 versions expressed from their endogenous promoter in *sac3Δ* cells. Sac3 localizes mainly to the nuclear periphery, where it exhibits a punctate staining pattern that is typical for NPCs and their associated proteins. Scale bar 3μm.

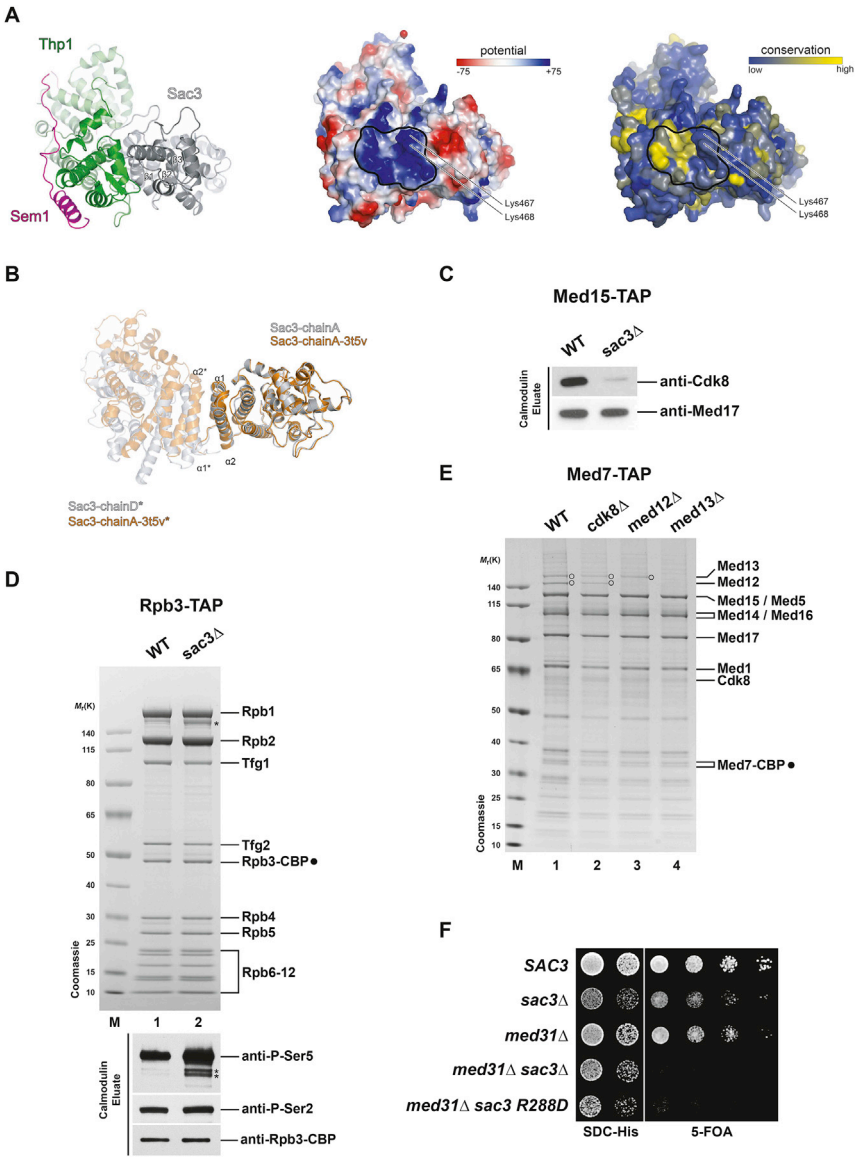

Figure S2. Structural, Biochemical, and Genetic Characterization of TREX-2, Mediator, and Pol II, Related to Figures 1 and 2

(A) Top view of the yeast Sac3(222-572)/Thp1(170-455)/Sem1 complex in ribbon representation, showing the electrostatic surface potential and the surface conservation of the trimeric complex (left to right). The winged-helix domains of Sac3 and Thp1 are encircled (black line). Positively charged Sac3 residues Lys467 and Lys468 that have been analyzed in mutational studies are indicated.

(B) Structural alignment of Sac3 from this study (gray) and Sac3 (PDB: 3t5v) (orange). The interaction of Sac3 with its crystallographic neighbor (*) is shown with α1 and α2 helices forming the crystallographic interface in both crystal forms.

(C) The yeast Mediator complex was affinity-purified via TAP-tagged Med15 from wild-type and *sac3Δ* cells. Calmodulin eluates were analyzed by SDS-PAGE and immunoblotting using the indicated antibodies. Loss of Cdk8 occurs also when Med15 is used as a TAP-tagged bait.

(D) Yeast RNA Polymerase II was affinity-purified via TAP-tagged Rpb3 from wild-type and *sac3Δ* cells. Calmodulin eluates were analyzed by SDS-PAGE and Coomassie staining (upper panel) and immunoblotting (lower panel) using the indicated antibodies. Subunits were assigned according to their calculated molecular weight. Tfg1 and Tfg2 are subunits of TFIIF. Asterisk indicates degradation product of Rpb1, which appeared to be more susceptible to proteolysis when hyperphosphorylated on Ser5.

(E) Med7-TAP purifications of Mediator from wild-type and mutant cells. Calmodulin eluates were analyzed by SDS-PAGE and Coomassie staining. Open circles indicate Med13 (top) and Med12 (bottom).

(F) Genetic interaction analysis shows negative synthetic links between *MED31* and *SAC3 R288D*. The indicated genotypes were produced by transformation with the respective HIS plasmids into cells which also contain a *SAC3* cover plasmid (URA3). Growth was followed on SDC-His and on SDC+5-fluoroorotic acid (5-FOA) plates to counterselect against the cover plasmid.

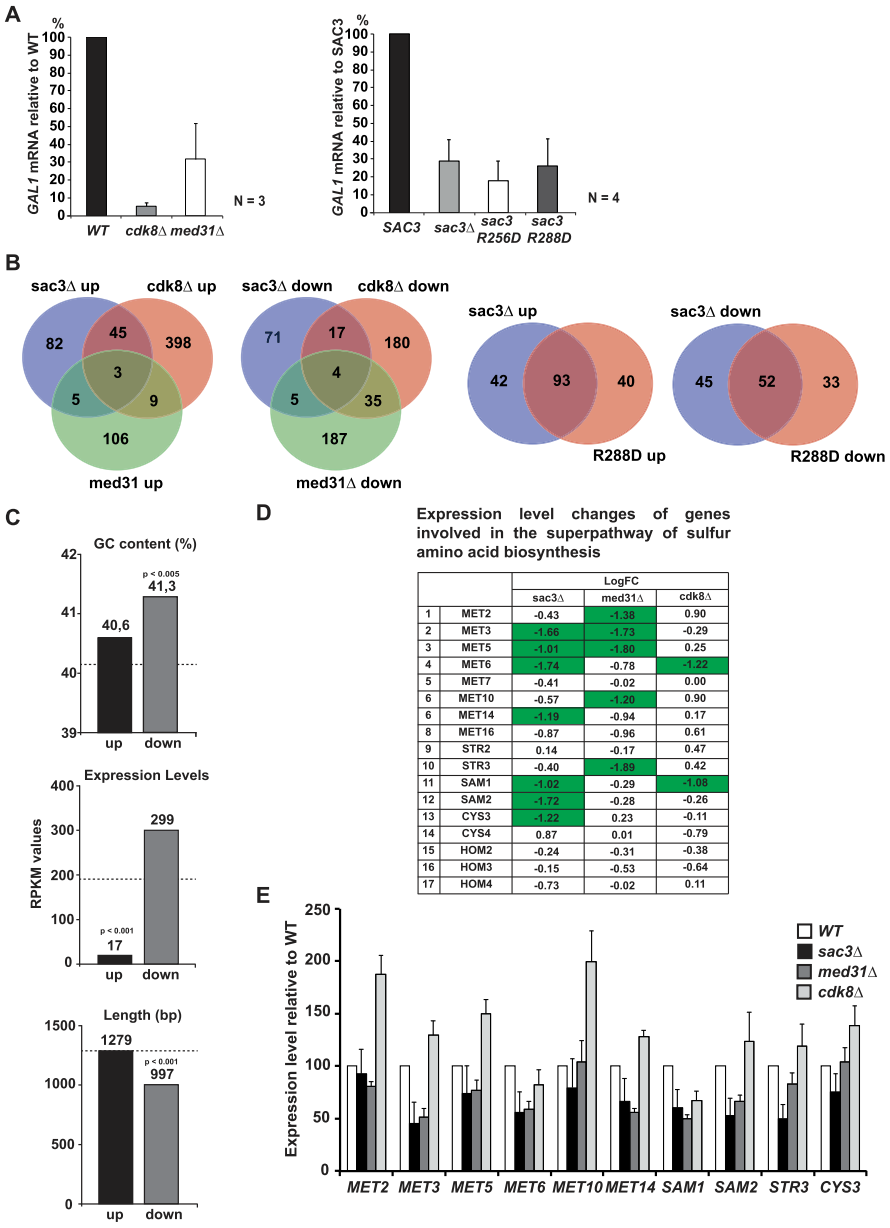

		LogFC		
		sac3Δ	med31Δ	cdk8Δ
1	MET2	-0.43	-1.38	0.90
2	MET3	-1.66	-1.73	-0.29
3	MET5	-1.01	-1.80	0.25
4	MET6	-1.74	-0.78	-1.22
5	MET7	-0.41	-0.02	0.00
6	MET10	-0.57	-1.20	0.90
6	MET14	-1.19	-0.94	0.17
8	MET16	-0.87	-0.96	0.61
9	STR2	0.14	-0.17	0.47
10	STR3	-0.40	-1.89	0.42
11	SAM1	-1.02	-0.29	-1.08
12	SAM2	-1.72	-0.28	-0.26
13	CYS3	-1.22	0.23	-0.11
14	CYS4	0.87	0.01	-0.79
15	HOM2	-0.24	-0.31	-0.38
16	HOM3	-0.15	-0.53	-0.64
17	HOM4	-0.73	-0.02	0.11

Figure S3. Gene Expression Analysis of TREX-2 and Mediator Mutants, Related to Figure 5

(A) *GAL1* activation in the indicated strains. Induction was performed by adding 2% galactose to raffinose-containing media and incubation for 60 min. Relative *GAL1* mRNA levels were analyzed by qPCR and normalized to *SCR1* RNA. Wild-type level was set to 100%. Error bars represent SD of three/four independent experiments as indicated. The qPCR primer sequences are listed in Table S2.

(B) Venn diagrams showing the number of overlapping and non-overlapping genes in *sac3Δ*, *cdk8Δ*, *med31Δ*, and *sac3* R288D mutant strains for up-and downregulated genes.

(C) Statistical analysis of G+C content, expression levels and gene length for up- and downregulated genes in *sac3Δ* cells. Mean values are shown; dashed line represents the genome mean. p values (Mann–Whitney's U-test) are indicated only for significant changes as compared to the genome mean. Downregulated genes in *sac3Δ* cells had a significantly higher GC content and were shorter in length than the genome average. Upregulated genes exhibited lower expression values than average.

(D) Table shows the expression level changes of genes involved in the superpathway of sulfur amino acid biosynthesis in the indicated mutants. Changes with a 2-fold or greater decrease in expression are marked in green. LogFC values for *med31Δ* cells were taken from Koschubs et al. (2009).

(E) Validation of target genes. mRNA levels of sulfur amino acid biosynthesis genes, which showed an at least 2-fold decrease in expression in one of the deletion mutants (labeled green in D) were measured by qPCR and normalized to *SCR1* RNA. Wild-type level was set to 100%. Error bars represent SD of three independent experiments. The qPCR primer sequences are listed in Table S2.

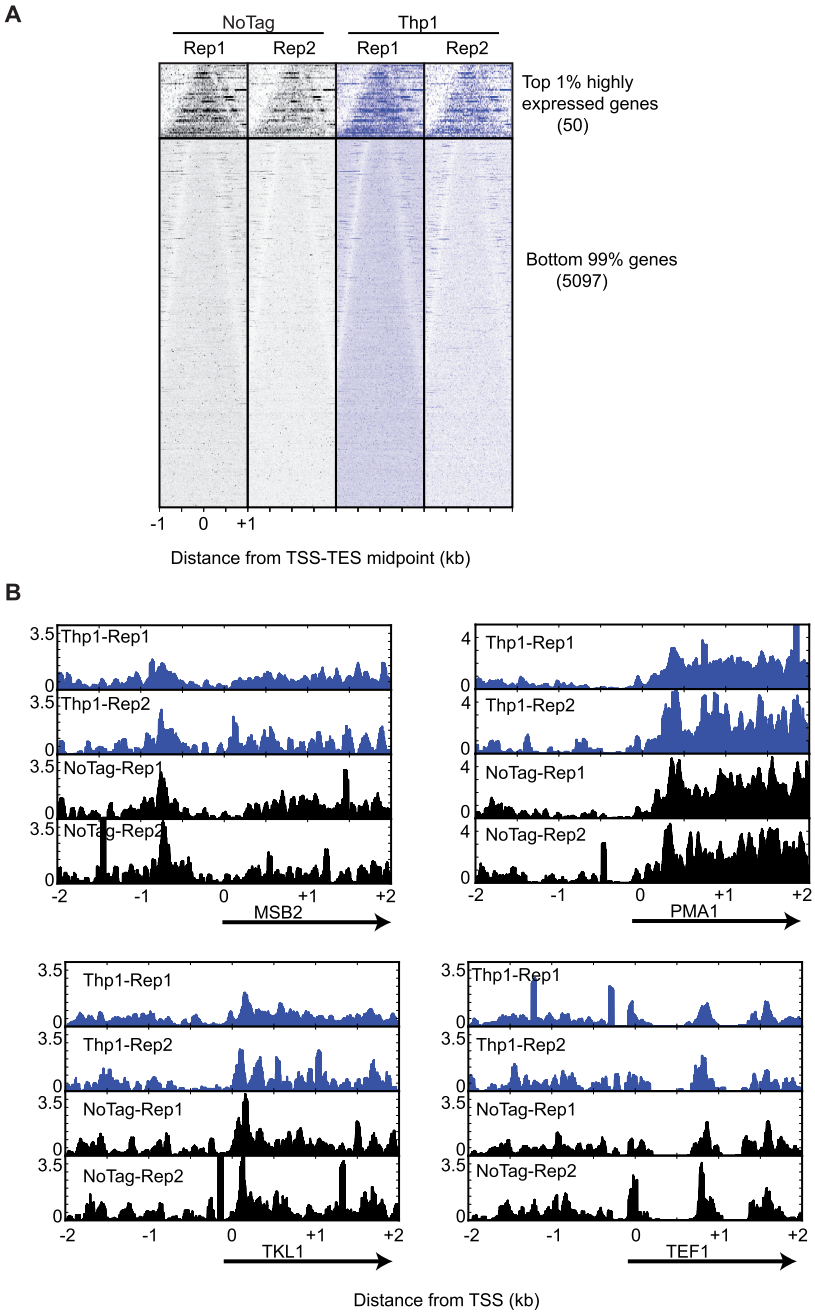

Figure S4. ChIP-exo of TREX-2, Related to Figure 5

(A) Comparison of ChIP-exo profiles for Thp1-TAP and NoTag control in two independent experiments showed no significant difference in Thp1 occupancy. Bell plots show 5′-end tags for Thp1 and noTag control, aligned by the midpoint of *t*ranscription *s*tart *s*ite (TSS) and *t*ranscription *e*nd *s*ite (TES) and sorted by the gene length. Upper and lower sets of panel correspond to top 1% highly expressed genes and the remaining 99% genes. Bell plots are a graphical way to analyze if a particular factor is enriched at the 5′ or 3′ end of genes or throughout the gene body. For every transcript defined by (Xu et al., 2009), the 5′ end of the sequencing reads (tags) were retrieved for a defined region (+/− 2kb) around the midpoint of transcription start site (TSS) and transcription end site (TES). After plotting the tags with respect to the TSS-TES midpoint, the genes are sorted based on transcript length which gives it a characteristic bell shape. Both NoTag and Thp1-TAP show enrichment in the gene body relative to the 5′/3′ end of genes.

(B) Plots of Thp1 and NoTag ChIP-exo reads over putative TREX-2 target genes featured in (Santos-Pereira et al., 2014). Shown is the smoothed distribution of ChIP-exo tags 5′ ends over a 4kb window around the TSS of *MSB2*, *PMA1*, *TKL1*, and *TEF1*. All datasets were normalized to have an equal number of tags.

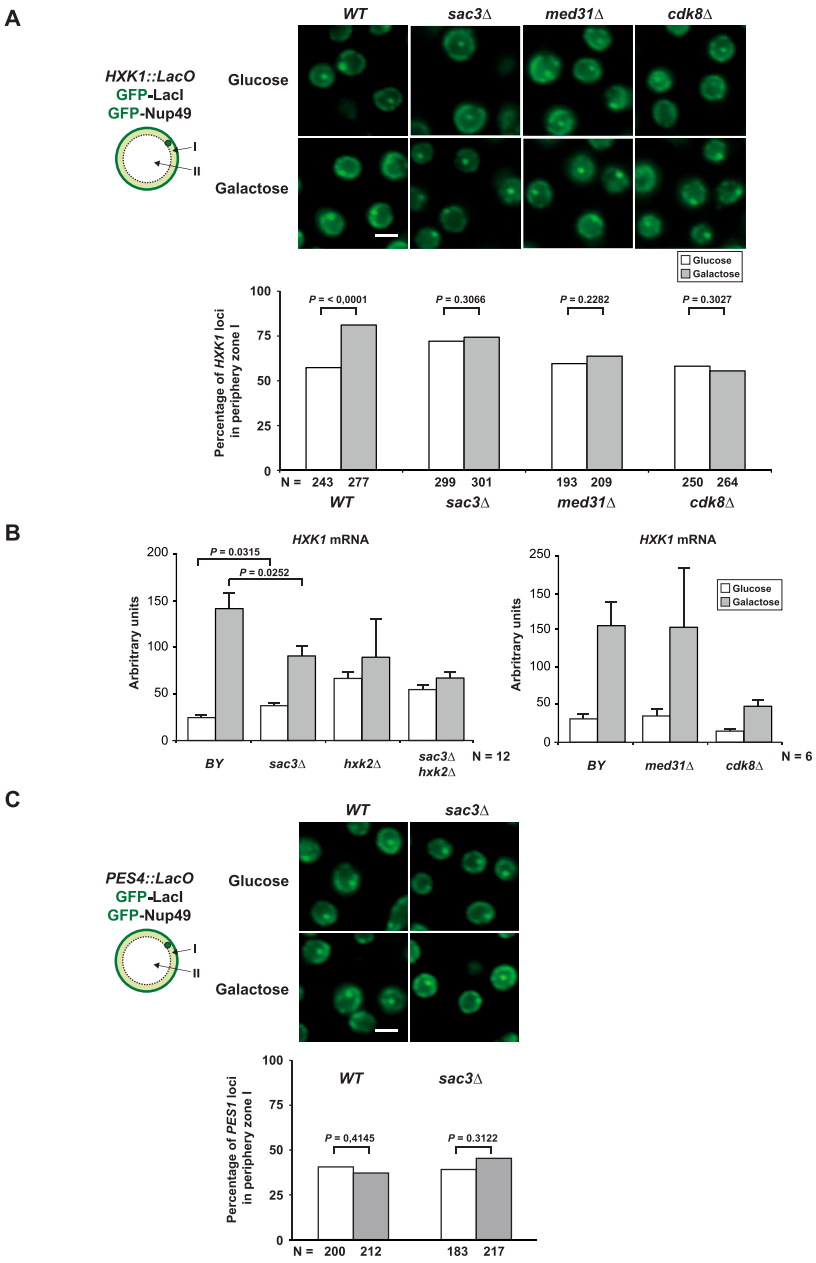

Figure S5. Gene-NPC Targeting and Expression of *HXK1*, Related to Figure 6

(A) *HXK1*-NPC targeting assay. Yeast cells expressing GFP–LacI and GFP–Nup49 fusions and carrying 256 lacO repeats upstream of the subtelomeric *HXK1* gene (Taddei et al., 2006) were analyzed under repressed (Glucose) and activated (Galactose) conditions in the respective strains. The percentage of *HXK1* loci in the nuclear periphery is indicated. N indicates the total number of cells analyzed. P-values refer to a one-tailed Fisher's exact test comparing the indicated distributions (scale bar, 2 μm).

(B) *HXK1* mRNA levels of uninduced (glucose) and induced (galactose) wild-type and indicated deletion strains. For *HXK1* induction an exponentially growing YPD culture was washed once in YPG and incubated for additional 60 min at 30°C in YPG. Quantification was performed by qPCR and normalized to *SCR1* RNA. Error bars represent SD of N independent biological replicates as indicated. Note that *SAC3* deletion causes a modest derepression of *HXK1* already in uninduced cells, which may correlate with a higher percentage of *HXK1* loci at the nuclear periphery (*WT* uninduced versus *sac3Δ* uninduced: p = 0,0003) (see A). Deletion of the transcriptional repressor *HXK2* induced *HXK1* transcription already in Glucose but could not recover gene expression to *WT* levels in *sac3Δ* cells upon Galactose induction. qPCR primers used are listed in Table S2.

(C) *PES4* nuclear position is insensitive to galactose (Taddei et al., 2006) or *SAC3* deletion. A strain bearing lacO repeats near *PES4* and expressing GFP-LacI and GFP-Nup49 was grown in glucose or galactose and compared to a *sac3Δ* mutant. The same analysis was performed as in (A).

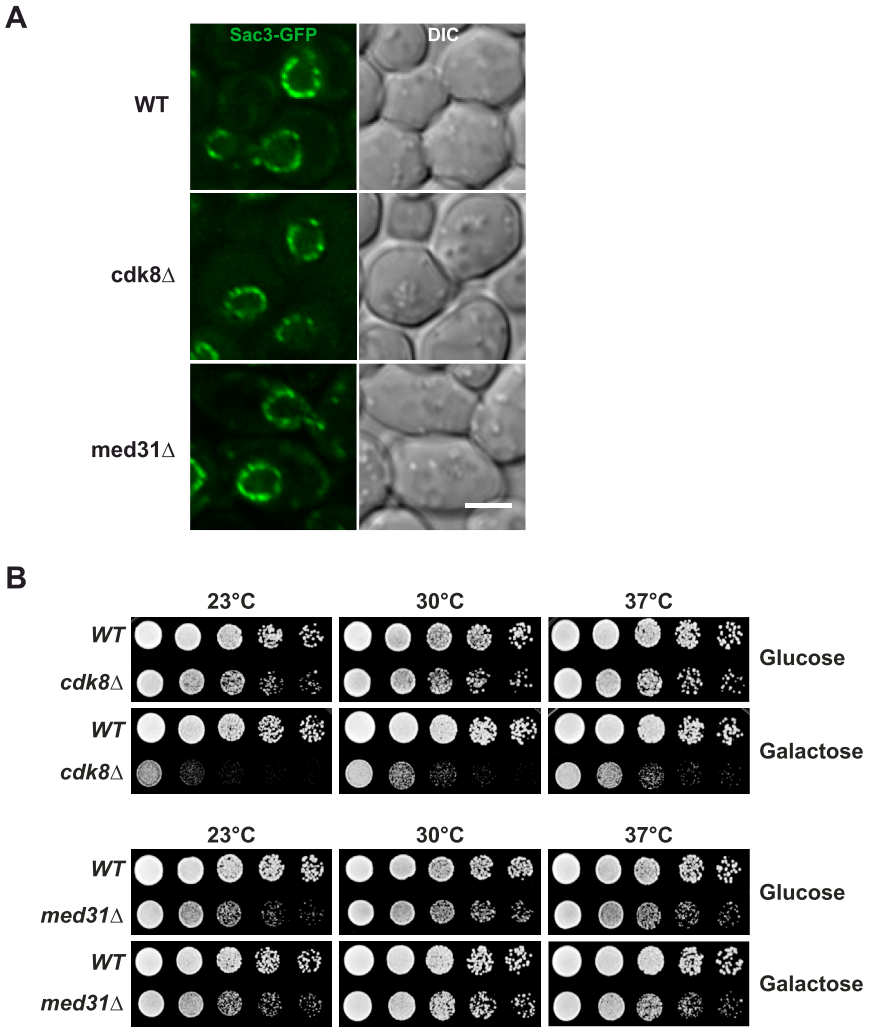

Figure S6. Sac3 Localization and Cell Growth in Mediator Mutants, Related to Figure 6

(A) Localization of N-terminally GFP-tagged wild-type Sac3 expressed from endogenous promoter in *sac3Δ* cells or cells carrying an additional deletion of *CDK8* or *MED31*. Sac3 localizes mainly to the nuclear periphery, where it exhibits a punctate staining pattern that is typical for NPCs and their associated proteins. Scale bar 3μm.

(B) Growth analyses of the indicated strains on medium prepared with glucose or galactose and different temperatures. Cell density was normalized and cells were spotted onto plates in 10-fold serial dilutions. Plates were incubated for 2-3 days.

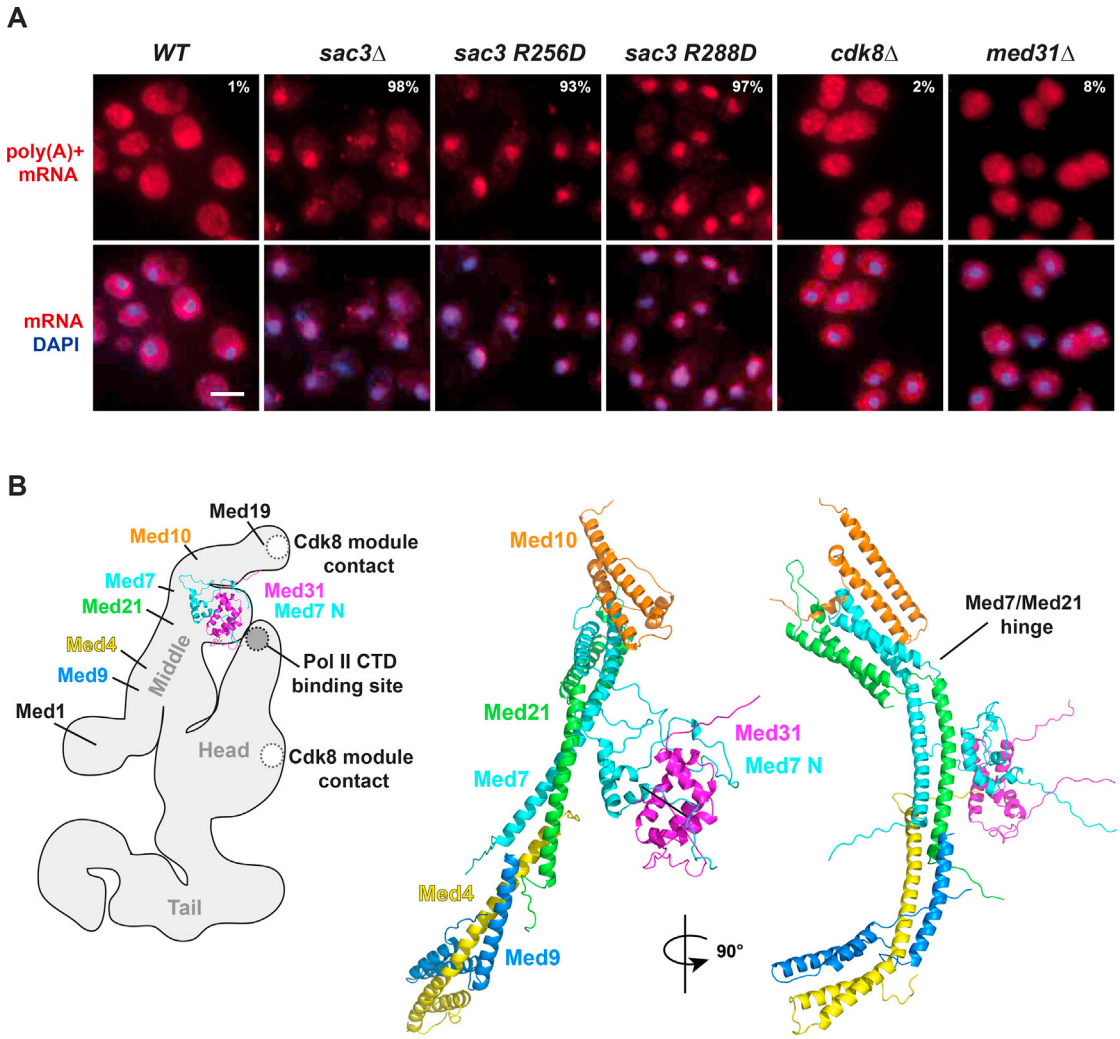

Figure S7. mRNA FISH Analysis and Model of the Mediator Middle Module, Related to Figures 3, 4, and 5

(A) Analysis of nuclear mRNA export in the indicated wild-type and mutant strains, containing the respective plasmids. Exponentially growing cells were subjected to poly(A)$^+$ RNA fluorescent in situ hybridization (FISH) with Cy3-labeled oligo probes. DNA was stained with DAPI. Percentage numbers indicate cells with nuclear fluorescent intensity above cytoplasmic signal (n = 100). Scale bar, 4 μm.

(B) Left: cartoon of the yeast Mediator complex cryo-EM structure (Tsai et al., 2014). Subunits of the 'middle' module are indicated based on the deletion, labeling, and crystal structure docking analysis performed in that study. Approximate positions of the Pol II CTD binding site (Robinson et al., 2012; Tsai et al., 2014) and two prominent Cdk8 kinase module contact points (Tsai et al., 2013) are marked. Right: structural model of yeast Mediator 'middle' module (Lariviere et al., 2013). The Med31/Med7N submodule in the left structure has the same orientation as the submodule docked into the cryo-EM based cartoon. Note that the Med31 submodule is flexibly connected to the elongated 'middle' backbone, which itself contains a conserved flexible hinge (Baumli et al., 2005). TREX-2 docking onto the Med31 submodule is proposed to induce conformational changes in this part of Mediator.

Cell

Supplemental Information

The Nuclear Pore-Associated TREX-2 Complex Employs Mediator to Regulate Gene Expression

Maren Schneider, Doris Hellerschmied, Tobias Schubert, Stefan Amlacher, Vinesh Vinayachandran, Rohit Reja, B. Franklin Pugh, Tim Clausen, and Alwin Köhler

Supplemental Information

Supplemental Experimental Procedures

Diffraction data processing, structure solution and analysis

Molecular replacement was performed with PHASER (McCoy et al., 2007). Model rebuilding and refinement proceeded in several cycles using the programs COOT (Emsley and Cowtan, 2004), O (Jones et al., 1991), CNS (Brunger et al., 1998) and Phenix (Adams et al., 2002). Ramachandran statistics were calculated with PROCHECK (Laskowski et al., 1993) and crystal contacts were analyzed with PISA (Krissinel and Henrick, 2007). Illustrations of the molecular structures were prepared with Pymol (DeLano, 2002), primary sequence alignments with Espript (Gouet et al., 1999). The sequence alignments for generating the surface conservation map were done with T-Coffee (Notredame et al., 2000).

Gene localization experiments

The *GAL1* locus was tagged with TetO repeats. The TetO array was labelled with TetR–GFP, the nuclear envelope with GFP–Nup188, and the labels were observed simultaneously *in vivo.* The fluorescently labeled *HXK1* and *PES1* genes are based on previously published strains (Taddei et al., 2006). Following induction, the exponentially growing cells were immobilized on agarose pads (2% agarose supplied with 2% glucose or galactose) for visualization. Sixteen *Z*-stacks with 200nm spacing were taken for each field. Image acquisition and subsequent deconvolution was carried out using softWoRx 6.0 software (GE Healthcare). The position of the labeled gene locus was determined in those cells where the brightest gene signal and the largest nuclear diameter were in the same *Z*-section. The nuclear volume was

divided in two equal volumes with a peripheral zone I and an interior zone II. Comparisons of gene locus distributions, computed for each strain and growth condition, were performed using the one-tailed Fisher's exact test.

mRNA quantification

Total RNA was extracted from 8mL of an exponentially growing culture using the hot phenol method as described earlier (Manuel Llinas, DeRisi Lab 2001; http://derisilab.ucsf.edu/microarray/protocols.html). cDNA was synthesized from 1µg of RNA using a cDNA synthesis kit (Promega) and analyzed by real-time PCR. Amount of mRNA was normalized to *SCR1*. Primers used for qPCR are listed in Table S2.

ChIP assay

Chromatin immunoprecipitation was done essentially as described before (van Attikum et al. 2004) with the following modifications: Formaldehyde fixation was performed at 22°C for 10 min. After sonication the protein amount was quantified via Bradford assay and equal amounts of cell lysate were used per IP. Upon incubation of lysate with antibody-coated magnetic beads, the beads were washed twice with lysis buffer, twice with lysis buffer containing 500mM NaCl, twice with wash buffer and once with TE. Chromatin was eluted with ChIP elution buffer (50mM Tris-HCl, pH 8.0; 10mM EDTA; 1% SDS). Occupancy of PolII at *GAL1* gene and Telomere control region was analyzed by real-time PCR.

ChIP-exo

Cells were grown in rich media and subjected to formaldehyde crosslinking, then processed through the ChIP-exo assay (Rhee and Pugh, 2011). Briefly, cells were disrupted, and chromatin pellets were isolated and then solubilized and fragmented by sonication. Immunoprecipitation was performed on fragmented chromatin from C-terminally TAP-tagged Thp1 or untagged control cells using magnetic beads conjugated with rabbit IgGs (Sigma I5006). After washing the beads to remove unbound proteins and DNA, and while still on the beads, the immunoprecipitates were polished, A-tailed, and ligated to an appropriate sequencing library adaptor. Samples were then subjected to

lambda exonuclease digestion, which processively removes nucleotides from 5′ ends of double-stranded DNA until blocked by a protein-DNA crosslink induced by formaldehyde treatment. The result is single-stranded DNA, which was then eluted from the magnetic beads and converted to double-stranded DNA by primer annealing and extension. A second sequencing adaptor was then ligated to exonuclease treated ends, then PCR amplified, gel purified, and sequenced. The complete ChIP-exo data are available at NCBI SRA (http://www.ncbi.nlm.nih.gov/sra) under the accession number SRA: SRP049207.

Transcriptome profiling

For RNA sequencing rRNA was removed from total RNA and cDNA libraries were generated using Ribo-zero Kit (Epicentre) and RNA ultra kit (NEB). Sequencing was performed on an Illumina HiSeq2000 platform. Reads were aligned against the *S. cerevisiae* reference genome (Ensembl R64-1-1 release) using TopHat version 2.0.9. After alignment reads were associated with known genes based on annotations derived from Ensembl and number of reads aligned with each gene was counted using Hiseq tool version 0.5.4p3. Data were normalized using TMM normalization method of the edgeR R/Bioconductor package (R version 3.0.1, Bioconductor version 2.12). For statistical analysis data were log transformed using voom approach in the limma package. For visualization and result files the TMM normalized counts are represented as RPKM values. All bioinformatical and statistical analysis were performed using limma package for R. GO Term analysis were done with topGO and GAGE packages. GC content, and gene length were extracted from the reference genome (Ensembl R64-1-1 release) and compared to the genome mean. For expression level analysis of RNAseq data, mean RPKM values of up or down regulated genes were calculated and compared to the genome mean. Transcriptome data of *med31*Δ cells was extracted from (Koschubs et al., 2009) Supplementary Table IVB. This previous analysis was performed in the same strain background as our mutants (BY), grown in the same condition (synthetic medium at 30°C) and analyzed with the same FDR (<0.05). The thresholds used for comparing all differentially expressed genes were logFC>1 (up-regulated) or logFC<-1

(down-regulated). The RNAseq data were uploaded to GEO (http://www.ncbi.nlm.nih.gov/geo/) under the accession number GEO: GSE67431.

Immunoblotting

The following antibodies were used in this study: α-Cdk8 (R. Young, MIT), α-Med17 (Y. Takagi, Indiana University), α-CBP (Thermo Scientific), α-Protein A and α-FLAG (SIGMA), α-Rpb1 CTD (Covance, Clone: 8WG16), α-Ser5-P (Cell Signaling, Clone: 4H8), α-Ser2-P (Clone: 3E10) and α-myc (Millipore).

Supplemental Figure Legends

Figure S1. Sac3 sequence analysis and characterization of Sac3 mutants, Related to Figure 1.

(A) Sequence alignment of Sac3 proteins from *S. cerevisiae, S. pombe, C. elegans, D. melanogaster, G. gallus, D. rerio, M. musculus,* and *H. sapiens*. Conserved residues are highlighted in boxes. Strictly conserved residues have a red background. Filled triangles mark strictly conserved residues located within clusters A and B of the Sac3 helical domain. Open triangles label residues Lys467 and Lys468, which are also shown in **Figure S2A**. Solid grey bar indicates sequence that defines the Sac3 PCI domain as 'atypical' compared to conventional PCI domain variants (Pick et al., 2009).

(B) SDS-PAGE analysis of 6His-Sac3 wild-type and mutant PCI domain complexes after polycistronic expression in *E. coli*, Ni-NTA affinity purification and size-exclusion chromatography on a Superdex 200 column.

(C) TREX-2 purification from yeast cells. Thp1-TAP sac3Δ strains were transformed with the indicated N-terminally myc-tagged *SAC3* plasmids (endogenous promoter) and subject to tandem-affinity purification. The full-length Sac3 protein typically shows variable signs of degradation. Sus1 and Cdc31 bind to the C-terminal domain of TREX-2 (see **Figure 1A**) and their stoichiometry with respect to Thp1 is a good proxy of overall complex integrity.

(D) Localization of N-terminally GFP-tagged Sac3 versions expressed from their endogenous promoter in *sac3*Δ cells. Sac3 localizes mainly to the

nuclear periphery, where it exhibits a punctate staining pattern that is typical for NPCs and their associated proteins. Scale bar 3µm.

Figure S2. Structural, biochemical and genetic characterization of TREX-2, Mediator and Pol II, Related to Figures 1 and 2.

(A) Top view of the yeast Sac3(222-572)/Thp1(170-455)/Sem1 complex in ribbon representation, showing the electrostatic surface potential and the surface conservation of the trimeric complex (left to right). The winged-helix domains of Sac3 and Thp1 are encircled (black line). Positively charged Sac3 residues Lys467 and Lys468 that have been analyzed in mutational studies are indicated.

(B) Structural alignment of Sac3 from this study (grey) and Sac3$_{3t5v}$. The interaction of Sac3 with its crystallographic neighbor (*) is shown with α1 and α2 helices forming the crystallographic interface in both crystal forms.

(C) The yeast Mediator complex was affinity-purified via TAP-tagged Med15 from wild-type and *sac3Δ* cells. Calmodulin eluates were analyzed by SDS-PAGE and immunoblotting using the indicated antibodies. Loss of Cdk8 occurs also when a different TAP-tagged bait is used.

(D) Yeast RNA Polymerase II was affinity-purified via TAP-tagged Rpb3 from wild-type and sac3Δ cells. Calmodulin eluates were analyzed by SDS-PAGE and Coomassie staining (upper panel) and immunoblotting (lower panel) using the indicated antibodies. Subunits were assigned according to their calculated molecular weight. Tfg1 and Tfg2 are subunits of TFIIF. Asterisk indicates degradation product of Rpb1, which appeared to be more susceptible to proteolysis when hyperphosphorylated on Ser5.

(E) Med7-TAP purifications of Mediator from wild-type and mutant cells. Calmodulin eluates were analyzed by SDS-PAGE and Coomassie staining. Open circles indicate Med13 (top) and Med12 (bottom).

(F) Genetic interaction analysis shows negative synthetic links between *MED31* and *SAC3 R288D*. The indicated genotypes were produced by transformation with the respective HIS plasmids into cells which also contain a *SAC3* cover plasmid (URA3). Growth was followed on SDC-His and on SDC+5-fluoroorotic acid (5-FOA) plates to counterselect against the cover plasmid.

Figure S3. Gene expression analysis of TREX-2 and Mediator mutants, Related to Figure 5.

(A) *GAL1* activation in the indicated strains. Induction was performed by adding 2% galactose to raffinose-containing media and incubation for 60 min. Relative *GAL1* mRNA levels were analyzed by qPCR and normalized to *SCR1* RNA. Wild-type level was set to 100%. Error bars represent standard deviation of three/four independent experiments as indicated. The qPCR primer sequences are listed in **Table S2**.

(B) Venn diagrams showing the number of overlapping and non-overlapping genes in *sac3*Δ, *cdk8*Δ, *med31*Δ and *SAC3 R288D* mutant strains for up-and down-regulated genes.

(C) Statistical analysis of G+C content, expression levels and gene length for up- and down-regulated genes in *sac3Δ* cells. Mean values are shown; dashed line represents the genome mean. P-values (Mann–Whitney's U-test) are indicated only for significant changes as compared to the genome mean. Down-regulated genes in *sac3*Δ cells had a significantly higher GC content and were shorter in length than the genome average. Up-regulated genes exhibited lower expression values than average.

(D) Table shows the expression level changes of genes involved in the superpathway of sulfur amino acid biosynthesis in the indicated mutants. Changes with a two-fold or greater decrease in expression are marked in green. LogFC values for *med31*Δ cells were taken from (Koschubs et al., 2009).

(E) Validation of target genes. mRNA levels of sulfur amino acid biosynthesis genes, which showed an at least two-fold decrease in expression in one of the deletion mutants (labeled green in **S3D**) were measured by qPCR and normalized to *SCR1* RNA. Wild-type level was set to 100%. Error bars represent standard deviation of three independent experiments. The qPCR primer sequences are listed in **Table S2**.

Figure S4. ChIP-exo of TREX-2, Related to Figure 5.

(A) Comparison of ChIP-exo profiles for Thp1-TAP and NoTag control in two independent experiments showed no significant difference in Thp1 occupancy.

Bell plots show 5'-end tags for Thp1 and noTag control, aligned by the midpoint of Transcription Start Site (TSS) and Transcription End Site (TES) and sorted by the gene length. Upper and lower sets of panel correspond to top 1% highly expressed genes and the remaining 99% genes. Bell plots are a graphical way to analyze if a particular factor is enriched at the 5' or 3' end of genes or throughout the gene body. For every transcript defined by (Xu et al., 2009), the 5' end of the sequencing reads (tags) were retrieved for a defined region (+/- 2kb) around the midpoint of transcription start site (TSS) and transcription end site (TES). After plotting the tags with respect to the TSS-TES midpoint, the genes are sorted based on transcript length which gives it a characteristic bell shape. Both NoTag and Thp1-TAP show enrichment in the gene body relative to the 5'/3' end of genes.

(B) Plots of Thp1 and NoTag ChIP-exo reads over putative TREX-2 target genes featured in (Santos-Pereira et al., 2014). Shown is the smoothed distribution of ChIP-exo tags 5' ends over a 4kb window around the TSS of *MSB2*, *PMA1*, *TKL1*, and *TEF1*. All datasets were normalized to have an equal number of tags.

Figure S5. Gene-NPC targeting and expression of *HXK1*, Related to Figure 6.

(A) *HXK1*-NPC targeting assay. Yeast cells expressing GFP–LacI and GFP–Nup49 fusions and carrying 256 lacO repeats upstream of the subtelomeric *HXK1* gene (Taddei et al., 2006) were analyzed under repressed (Glucose) and activated (Galactose) conditions in the respective strains. The percentage of *HXK1* loci in the nuclear periphery is indicated. N indicates the total number of cells analyzed. P-values refer to a one-tailed Fisher's exact test comparing the indicated distributions (scale bar, 2 μm).

(B) *HXK1* mRNA levels of uninduced (Glucose) and induced (Galactose) wild-type and indicated deletion strains. For *HXK1* induction an exponentially growing YPD culture was washed once in YPG and incubated for additional 60 min at 30°C in YPG. Quantification was performed by qPCR and normalized to *SCR1* RNA. Error bars represent standard deviation of N independent biological replicates as indicated. Note that *SAC3* deletion causes a modest derepression of *HXK1* already in uninduced cells, which

may correlate with a higher percentage of HXK1 loci at the nuclear periphery (*WT* uninduced vs. *sac3*Δ uninduced: *P*= 0,0003) (see **Figure S5A)**. Deletion of the transcriptional repressor *HXK2* induced *HXK1* transcription already in Glucose but could not recover gene expression to *WT* levels in *sac3*Δ cells upon Galactose induction. qPCR primers used are listed in **Table S2**.

(C) *PES4* nuclear position is insensitive to galactose (Taddei et al., 2006) or *SAC3* deletion. A strain bearing lacO repeats near *PES4* and expressing GFP-LacI and GFP-Nup49 was grown in glucose or galactose and compared to a *sac3*Δ mutant. The same analysis was performed as in (**A**).

Figure S6. Sac3 localization and cell growth in Mediator mutants, Related to Figure 6.

(A) Localization of N-terminally GFP-tagged wild-type Sac3 expressed from endogenous promoter in *sac3*Δ cells or cells carrying an additional deletion of *CDK8* or *MED31*. Sac3 localizes mainly to the nuclear periphery, where it exhibits a punctate staining pattern that is typical for NPCs and their associated proteins. Scale bar 3µm.

(**B**) Growth analyses of the indicated strains on medium prepared with glucose or galactose and different temperatures. Cell density was normalized and cells were spotted onto plates in 10-fold serial dilutions. Plates were incubated for 2-3 days.

Figure S7. mRNA FISH analysis and model of the Mediator middle module.

(A) Analysis of nuclear mRNA export in the indicated wild-type and mutant strains, containing the respective plasmids. Exponentially growing cells were subjected to poly(A)+ RNA fluorescent *in situ* hybridization (FISH) with Cy3-labeled oligo probes. DNA was stained with DAPI. Percentage numbers indicate cells with nuclear fluorescent intensity above cytoplasmic signal (n=100). Scale bar, 4 µm.

(B) On the left: Cartoon of the yeast Mediator complex cryo-EM structure (Tsai et al., 2014). Subunits of the ‘middle‘ module are indicated based on the deletion, labeling and crystal structure docking analysis performed in that study. Approximate positions of the Pol II CTD binding site (Robinson et al.,

2012; Tsai et al., 2014) and two prominent Cdk8 kinase module contact points (Tsai et al., 2013) are marked. On the right: Structural model of yeast Mediator ‘middle‘ module (Lariviere et al., 2013). The Med31/Med7N submodule in the left structure has the same orientation as the submodule docked into the cryo-EM based cartoon. Note that the Med31 submodule is flexibly connected to the elongated ‘middle‘ backbone, which itself contains a conserved flexible hinge (Baumli et al., 2005). TREX-2 docking onto the Med31 submodule is proposed to induce conformational changes in this part of Mediator.

Table S1. Data collection and refinement statistics for PDB: 4trq, Related to Figure 1.

Space Group	
Space group	$P4_12_12$
Cell dimensions *a*, *b*, *c* (Å)	125.7, 125.7, 268.4
Data collection	
Wavelength (Å)	0.979
Resolution (Å)	47.6-3.1
R_{sym}(%)	11.5 (74.3)
I /sigma(*I*)	10.4 (2)
Completeness (%)	99.0 (99.9)
Redundancy	4.4 (4.6)
Refinement	
Resolution (Å)	47.6-3.1
No. of reflections	39,366
R_{work}/R_{free}(%)	19.4/23.8
No. atoms	
Protein	10,516
Ligand	5
B-factors	
Protein	76.1
Ligand	94.6
R.m.s deviations	
Bond lengths (Å)	0.008
Bond angles (º)	1.27
Ramachandran statistics (%)	
most favored regions	87.5
additional allowed regions	11.5
generously allowed regions	0.4
disallowed regions	0.5

The structure was deposited under PDB: 4trq.

Table S2. List of primers used in this study, Related to experimental methods.

Primers used for RT-qPCR	
GAL1 mRNA FW	5'-TGAAGAGTCTCTCGCCAATAAGAA-3'
GAL1 mRNA RV	5'-TCGCGAGAACAATTCAAGGA-3'
SCR1 RNA FW	5'-CTTTCTGGTGGGATGGGATA-3'
SCR1 RNA RV	5'-CACGGTGCGGAATAGAGAAC-3'
HXK1 mRNA FW	5'-CGGTTGGGTCATGGAATTCC-3'
HXK1 mRNA RV	5'-GGTTACCGCTCAACTTGACC-3'
MET2 mRNA FW	5'-ACCAGGGCACAAAGTTCATC-3'
MET2 mRNA RV	5'-TACCGATGATCAGGGATGGT-3'
MET3 mRNA FW	5'-GCCCTTTTCCAAGATGATGA-3'
MET3 mRNA RV	5'-CTGGATGTTCTGGGTCACCT-3'
MET5 mRNA FW	5'-AATGACTGGTTGCCCTAACG-3'
MET5 mRNA RV	5'-TAACCACCACCAAGCATCAA-3'
MET6 mRNA FW	5'-TCGGTACCGTTGTCCCTAAC-3'
MET6 mRNA RV	5'-CCAACGGACAAGGTTTGTTT-3'
MET10 mRNA FW	5'-ACGACGAGTCCAAATTGTCC-3'
MET10 mRNA RV	5'-GCTGAAATGTCTGCACCTGA-3'
MET14 mRNA FW	5'-ACGCAAGGCATTGAGAAAAC-3'
MET14 mRNA RV	5'-CGAATGTTGTCACCATCCAA-3'
SAM1 mRNA FW	5'-TACTGCGACCAAGTCTGACG-3'
SAM1 mRNA RV	5'-AGAAGCGGTTGGCAAGTAGA-3'
SAM2 mRNA FW	5'-TCGACTTGAGACCAGGTGTG-3'
SAM2 mRNA RV	5'-TCTTTGGTTTTTCCCATGAGT-3'
STR3 mRNA FW	5'-ATCGTGTCCCACAGGAAAAC-3'

STR3 mRNA RV	5'-ATCGCCGGCTATTATTGTTG-3'
CYS3 mRNA FW	5'-CTTGGTTGACCCACAGAGGT-3'
CYS3 mRNA RV	5'-CTGGGTAGTTGACTGCGACA-3'
Primers used for ChIP analysis	
GAL1 promoter FW	5'-TCCGAACAATAAAGATTCTACAA-3'
GAL1 promoter RV	5'-CGCATTATCATCCTATGGTT-3'
GAL1 5'ORF FW	5'-CCTGAGTTCAATTCTAGCGCA-3'
GAL1 5'ORF RV	5'-ACTCTACCAGGCGATCTAGC-3'
GAL1 3'ORF FW	5'-TGGGGTGGTTGTACTGTTCA-3'
GAL1 3'ORF RV	5'-TCAGCATCAGTGATCTTAGGGT-3'
GAL1 3'UTR FW	5'-ACTTTAGCATCACAAAATACGCA-3'
GAL1 3'UTR RV	5'-CCCTGTGTTTTAAAGTTTGTGGA-3'
TEL06 FW	5'-GCTGAAGTTTAACGGTGATTATTAGG-3'
TEL06 RV	5'-TGGCCTCACTGGTTTTTACC-3'

Table S3*. S. cerevisiae* strains used in this study, Related to experimental methods.

Name	Genotype	Reference
BY4741	*MATa; his3Δ1; leu2Δ0; met15Δ0; ura3Δ0*	EUROSCARF
*sac3*Δ	*MATa; his3Δ1; leu2Δ0; met15Δ0; ura3Δ0 sac3Δ::kanMX4*	EUROSCARF
*cdk8*Δ	*MATa; his3Δ1; leu2Δ0; met15Δ0; ura3Δ0 cdk8Δ::kanMX4*	EUROSCARF
*med31*Δ	*MATa; his3Δ1; leu2Δ0; met15Δ0; ura3Δ0 med31Δ::natNT2*	This study
*med1*Δ	*MATa; his3Δ1; leu2Δ0; met15Δ0; ura3Δ0 med1Δ::natNT2*	This study
*med5*Δ	*MATa; his3Δ1; leu2Δ0; met15Δ0; ura3Δ0 med5Δ::natNT2*	This study
*med9*Δ	*MATa; his3Δ1; leu2Δ0; met15Δ0; ura3Δ0 med9Δ::natNT2*	This study
*sac3*Δ *cdk8*Δ shuffle strain	*MATa; his3Δ1; leu2Δ0; met15Δ0; ura3Δ0 sac3Δ::kanMX4 cdk8*Δ*::natNT2 pRS316-SAC3*	This study
*sac3*Δ *med31*Δ shuffle strain	*MATa; his3Δ1; leu2Δ0; met15Δ0; ura3Δ0 sac3Δ::kanMX4 med31*Δ*::natNT2*	This study

	pRS316-SAC3	
*sac3*Δ *med1*Δ shuffle strain	*MATa; his3Δ1; leu2Δ0; met15Δ0; ura3Δ0 sac3Δ::kanMX4 med1*Δ*::natNT2 pRS316-SAC3*	This study
*sac3*Δ *med5*Δ shuffle strain	*MATa; his3Δ1; leu2Δ0; met15Δ0; ura3Δ0 sac3Δ::kanMX4 med5*Δ*::natNT2 pRS316-SAC3*	This study
*sac3*Δ *med9*Δ shuffle strain	*MATa; his3Δ1; leu2Δ0; met15Δ0; ura3Δ0 sac3Δ::kanMX4 med9*Δ*::natNT2 pRS316-SAC3*	This study
*hxk2*Δ	*MATa; his3Δ1; leu2Δ0; met15Δ0; ura3Δ0* hxk2Δ::natNT2	This study
*sac3*Δ *hxk2*Δ	*MATa; his3Δ1; leu2Δ0; met15Δ0; ura3Δ0 sac3*Δ*::kan* hxk2Δ::natNT2	This study
MED7-TAP	*MATa; his3Δ1; leu2Δ0; met15Δ0; ura3Δ0 MED7-TAP::HIS3MX6*	Open Biosystems
*MED7-TAP sac3*Δ	*MATa; his3Δ1; leu2Δ0; met15Δ0; ura3Δ0 MED7-TAP::HIS3MX6 sac3*Δ*::natNT2*	This study
*MED7-TAP cdk8*Δ	*MATa; his3Δ1; leu2Δ0; met15Δ0; ura3Δ0 MED7-TAP::HIS3MX6 cdk8*Δ*::natNT2*	This study
*MED7-TAP med13*Δ	*MATa; his3Δ1; leu2Δ0; met15Δ0; ura3Δ0 MED7-TAP::HIS3MX6 med13*Δ*::natNT2*	This study
*MED7-TAP med12*Δ	*MATa; his3Δ1; leu2Δ0; met15Δ0; ura3Δ0 MED7-TAP::HIS3MX6 med12*Δ*::natNT2*	This study
*MED7-TAP med31*Δ	*MATa; his3Δ1; leu2Δ0; met15Δ0; ura3Δ0 MED7-TAP::HIS3MX6 med31*Δ*::natNT2*	This study
*MED7-TAP med1*Δ	*MATa; his3Δ1; leu2Δ0; met15Δ0; ura3Δ0 MED7-TAP::HIS3MX6 med1*Δ*::natNT2*	This study
*MED7-TAP med9*Δ	*MATa; his3Δ1; leu2Δ0; met15Δ0; ura3Δ0 MED7-TAP::HIS3MX6 med9*Δ*::natNT2*	This study
MED15-TAP	*MATa; his3Δ1; leu2Δ0; met15Δ0; ura3Δ0 MED15-TAP::HIS3MX6*	Open Biosystems
*MED15-TAP sac3*Δ	*MATa; his3Δ1; leu2Δ0; met15Δ0; ura3Δ0 MED15-TAP::HIS3MX6 sac3*Δ*::natNT2*	This study
RPB3-TAP	*MATa; his3Δ1; leu2Δ0; met15Δ0; ura3Δ0 RPB3-TAP::HIS3MX6*	Open Biosystems
*RPB3-TAP sac3*Δ	*MATa; his3Δ1; leu2Δ0; met15Δ0; ura3Δ0 RPB3-TAP::HIS3MX6 sac3*Δ*::natNT2*	This study
*THP1-TAP sac3*Δ	*MATa; his3Δ1; leu2Δ0; met15Δ0; ura3Δ0* THP1-TAP*::HIS3MX6 sac3*Δ*::natNT2*	This study
*YGCMS sac3*Δ	*MAT a, leu2, his3, trp1, ade2, ura3 LEU2::TetR-GFP::leu2, (tetO*112)-Nat::interGAL1-FUR4, NUP188-*	This study

	GFP::TRP1 sac3Δ::kanMX6	
YGCMS cdk8Δ	*MAT a, leu2, his3, trp1, ura3 LEU2::TetR-GFP::leu2, (tetO*112)-Nat::interGAL1-FUR4, NUP188-GFP::TRP1 cdk8Δ::kanMX6*	This study
YGCMS med31Δ	*MAT a, leu2, his3, trp1, ura3 LEU2::TetR-GFP::leu2, (tetO*112)-Nat::interGAL1-FUR4, NUP188-GFP::TRP1 med31Δ::kanMX6*	This study
GA-1459	*Nup49-GFP his3::lacI-GFP::HIS3 Telo6R (HXK1)::lacO-TRP1*	Taddei et al., 2006 Nature
GA-1459 sac3Δ	*Nup49-GFP his3::lacI-GFP::HIS3 Telo6R (HXK1)::lacO-TRP1 sac3Δ::natNT2*	This study
GA-1459 cdk8Δ	*Nup49-GFP his3::lacI-GFP::HIS3 Telo6R (HXK1)::lacO-TRP1 cdk8Δ::natNT2*	This study
GA-1459 med31Δ	*Nup49-GFP his3::lacI-GFP::HIS3 Telo6R (HXK1)::lacO-TRP1 sac3Δ::natNT2*	This study
GA-1461	*Nup49-GFP his3::lacI-GFP::HIS3 PES4::lacO-TRP1*	Taddei et al., 2006 Nature
GA-1461 sac3Δ	*Nup49-GFP his3::lacI-GFP::HIS3 PES4::lacO-TRP1 sac3Δ::natNT2*	This study

Table S4. Plasmids used in this study, Related to experimental methods.

Name	Relevant information	Reference
pRS313	*ARS/CEN HIS3*	(Sikorski and Hieter, 1989)
pRS313-MYC-SAC3#	*ARS/CEN HIS3 P_{SAC3}MYC-SAC3*	This study
pRS313-GFP-SAC3#	*ARS/CEN HIS3 P_{SAC3}GFP-SAC3*	This study
pRS315	*ARS/CEN LEU2*	(Sikorski and Hieter, 1989)
pRS315-MYC-SAC3#	*ARS/CEN LEU2 P_{SAC3}MYC-SAC3*	This study
pRS315-CDK8	*ARS/CEN LEU2 P_{CDK8}CDK8*	This study
pRS315-cdk8 D304A	*ARS/CEN LEU2 P_{CDK8}cdk8 D304A*	This study
pRS411	*ARS/CEN MET15*	(Brachmann et al., 1998)
pFA6a-natNT2	natNT2 for genomic deletion	(Janke et al., 2004)
pFA6a-kanMX6	kanMX6 for genomic deletion	(Longtine et al., 1998)
pST44 6HIS-TEV-SAC3aa222-572# THP1-FLAG SEM1	Ampicillin, Polycistronic expression in E.coli	This study. Based on the pST44 vector (Tan et al., 2005)

pST44 6HIS-TEV-SAC3aa222-572[#] THP1aa170-455 SEM1	Ampicillin, Polycistronic expression in E.coli	This study
pST44 GST-TEV-MED31 Med7aa1-83	Ampicillin, Polycistronic expression in E.coli	This study

[#] plasmids carrying mutant variants of *SAC3* were created by site-directed mutagenesis and verfied by sequencing

Table S5. Gene Ontology (GO) term analysis of deregulated genes in *sac3*Δ cells, Related to Figure 5.

List of significantly enriched GO terms. Only down-regulated genes were further analyzed. Genes in involved in yeast sexual conjugation scored highest among the up-regulated genes in *sac3*Δ.

Table S6. Mass spectrometry, Related to Figure 2.

Details of mass spectrometry analysis of a Med7-TAP purification. Coomassie-bands were cut individually from the gel and analyzed by microcapillary LC-MS/MS techniques on Orbitrap mass spectrometers (Thermo Scientific). Proteins with fewer than 10 unique peptides are excluded from the list. Bold protein names correspond to the bands that are assigned in **Figure 2A**. Note that peptides (fewer than 10) corresponding to Sac3 and the basket protein Nup60 were also identified in wild-type Mediator preparations. The Sac3 peptides are degradation products of the full-length protein (150 kDa).

Protein	Unique Peptides	Total Peptides
Med13	**55**	**107**
Med12	13	15
Med14	13	14

Med12	**44**	**58**
Med14	11	13
Med5	11	11

Med15	**59**	**136**
Med5	**64**	**197**
Med14	19	20
Med13	17	18
Rpb2	13	14

Med14	**53**	**120**
Med16	**46**	**133**
*Sac3	4	6

Med17	**52**	**115**
Hsp90	16	19
Med14	15	17
Med15	13	16

Med1	**39**	**163**
Hsp75	24	44
Med14	12	13
Pab1	11	14
*Nup60	3	6
*Sac3	2	3
Cdk8	**22**	**34**
Med2	11	17

Med3	**10**	**20**
Med15	10	12
Med1	10	10

Med4	34	138
Med6	32	89
Tdh1	10	20

Med18	**22**	**92**
Med7-CBP	**14**	**59**
Rpp0	12	31
Asc1	11	13
Med2	10	15

Med8	**21**	**61**
CycC (Ssn8)	**19**	**38**
Yra1	12	29
Med19	**10**	**23**

Med20	**13**	**88**

Med9	**17**	**64**
Med10	**16**	**62**
Med21	**14**	**98**
Rpl25	10	17

Med11	**15**	**57**
Med22	**10**	**46**
Hhf1	10	21

Supplemental References

DeLano, W.L. (2002). The Pymol Molecular Graphics System (San Carlos, CA: DeLano Scientific).

Adams, P.D., Grosse-Kunstleve, R.W., Hung, L.W., Ioerger, T.R., McCoy, A.J., Moriarty, N.W., Read, R.J., Sacchettini, J.C., Sauter, N.K., and Terwilliger, T.C. (2002). PHENIX: building new software for automated crystallographic

structure determination. Acta crystallographica Section D, Biological crystallography *58*, 1948-1954.

Baumli, S., Hoeppner, S., and Cramer, P. (2005). A conserved mediator hinge revealed in the structure of the MED7.MED21 (Med7.Srb7) heterodimer. The Journal of biological chemistry *280*, 18171-18178.

Brachmann, C.B., Davies, A., Cost, G.J., Caputo, E., Li, J., Hieter, P., and Boeke, J.D. (1998). Designer deletion strains derived from Saccharomyces cerevisiae S288C: a useful set of strains and plasmids for PCR-mediated gene disruption and other applications. Yeast *14*, 115-132.

Brunger, A.T., Adams, P.D., Clore, G.M., DeLano, W.L., Gros, P., Grosse-Kunstleve, R.W., Jiang, J.S., Kuszewski, J., Nilges, M., Pannu, N.S.*, et al.* (1998). Crystallography & NMR system: A new software suite for macromolecular structure determination. Acta crystallographica Section D, Biological crystallography *54*, 905-921.

Emsley, P., and Cowtan, K. (2004). Coot: model-building tools for molecular graphics. Acta crystallographica Section D, Biological crystallography *60*, 2126-2132.

Gouet, P., Courcelle, E., Stuart, D.I., and Metoz, F. (1999). ESPript: analysis of multiple sequence alignments in PostScript. Bioinformatics *15*, 305-308.

Janke, C., Magiera, M.M., Rathfelder, N., Taxis, C., Reber, S., Maekawa, H., Moreno-Borchart, A., Doenges, G., Schwob, E., Schiebel, E.*, et al.* (2004). A versatile toolbox for PCR-based tagging of yeast genes: new fluorescent proteins, more markers and promoter substitution cassettes. Yeast *21*, 947-962.

Jones, T.A., Zou, J.Y., Cowan, S.W., and Kjeldgaard, M. (1991). Improved methods for building protein models in electron density maps and the location of errors in these models. Acta crystallographica Section A, Foundations of crystallography *47 (Pt 2)*, 110-119.

Koschubs, T., Seizl, M., Lariviere, L., Kurth, F., Baumli, S., Martin, D.E., and Cramer, P. (2009). Identification, structure, and functional requirement of the Mediator submodule Med7N/31. The EMBO journal *28*, 69-80.

Krissinel, E., and Henrick, K. (2007). Inference of macromolecular assemblies from crystalline state. Journal of molecular biology *372*, 774-797.

Lariviere, L., Plaschka, C., Seizl, M., Petrotchenko, E.V., Wenzeck, L., Borchers, C.H., and Cramer, P. (2013). Model of the Mediator middle module based on protein cross-linking. Nucleic acids research *41*, 9266-9273.

Longtine, M.S., McKenzie, A., 3rd, Demarini, D.J., Shah, N.G., Wach, A., Brachat, A., Philippsen, P., and Pringle, J.R. (1998). Additional modules for versatile and economical PCR-based gene deletion and modification in Saccharomyces cerevisiae. Yeast *14*, 953-961.

McCoy, A.J., Grosse-Kunstleve, R.W., Adams, P.D., Winn, M.D., Storoni, L.C., and Read, R.J. (2007). Phaser crystallographic software. Journal of applied crystallography *40*, 658-674.

Notredame, C., Higgins, D.G., and Heringa, J. (2000). T-Coffee: A novel method for fast and accurate multiple sequence alignment. Journal of molecular biology *302*, 205-217.

Rhee, H.S., and Pugh, B.F. (2011). Comprehensive genome-wide protein-DNA interactions detected at single-nucleotide resolution. Cell *147*, 1408-1419.

Robinson, P.J., Bushnell, D.A., Trnka, M.J., Burlingame, A.L., and Kornberg, R.D. (2012). Structure of the mediator head module bound to the carboxy-terminal domain of RNA polymerase II. Proceedings of the National Academy of Sciences of the United States of America *109*, 17931-17935.

Santos-Pereira, J.M., Garcia-Rubio, M.L., Gonzalez-Aguilera, C., Luna, R., and Aguilera, A. (2014). A genome-wide function of THSC/TREX-2 at active genes prevents transcription-replication collisions. Nucleic acids research *42*, 12000-12014.

Sikorski, R.S., and Hieter, P. (1989). A system of shuttle vectors and yeast host strains designed for efficient manipulation of DNA in Saccharomyces cerevisiae. Genetics *122*, 19-27.

Taddei, A., Van Houwe, G., Hediger, F., Kalck, V., Cubizolles, F., Schober, H., and Gasser, S.M. (2006). Nuclear pore association confers optimal expression levels for an inducible yeast gene. Nature *441*, 774-778.

Tan, S., Kern, R.C., and Selleck, W. (2005). The pST44 polycistronic expression system for producing protein complexes in Escherichia coli. Protein expression and purification *40*, 385-395.

Tsai, K.L., Sato, S., Tomomori-Sato, C., Conaway, R.C., Conaway, J.W., and Asturias, F.J. (2013). A conserved Mediator-CDK8 kinase module association regulates Mediator-RNA polymerase II interaction. Nature structural & molecular biology *20*, 611-619.

Tsai, K.L., Tomomori-Sato, C., Sato, S., Conaway, R.C., Conaway, J.W., and Asturias, F.J. (2014). Subunit architecture and functional modular rearrangements of the transcriptional mediator complex. Cell *157*, 1430-1444.

Xu, Z., Wei, W., Gagneur, J., Perocchi, F., Clauder-Munster, S., Camblong, J., Guffanti, E., Stutz, F., Huber, W., and Steinmetz, L.M. (2009). Bidirectional promoters generate pervasive transcription in yeast. Nature *457*, 1033-1037.